

# 1 **Beyond trees: mapping total aboveground biomass density in the** 2 **Brazilian savanna using high-density UAV-lidar data**

3

4 Máira Beatriz Teixeira da Costa<sup>1</sup>, Carlos Alberto Silva<sup>2,3\*</sup>, Eben North Broadbent  
5 <sup>4</sup>Rodrigo Vieira Leite<sup>5</sup>, Midhun Mohan<sup>6</sup>, Veraldo Liesenberg<sup>7</sup>, Jaz Stoddart<sup>8</sup>, Cibele  
6 Hummel do Amaral<sup>5</sup>, Danilo Roberti Alves de Almeida<sup>9</sup>, Anne Laura da Silva<sup>10</sup>,  
7 Lucas Ruggeri Ré Y Goya<sup>10</sup>, Victor Almeida Cordeiro<sup>10</sup>, Franciel Rex<sup>11</sup>, Andre  
8 Hirsch<sup>10</sup>, Gustavo Eduardo Marcatti<sup>10</sup>, Adrian Cardil<sup>12,13,14</sup>, Bruno Araujo Furtado  
9 de Mendonça<sup>15</sup>, Caio Hamamura<sup>16</sup>, Ana Paula Dalla Corte<sup>11</sup>, Eraldo Aparecido  
10 Trondoli Matricardi<sup>1</sup>, Andrew T. Hudak<sup>17</sup>, Angelica Maria Almeyda Zambrano<sup>18</sup>,  
11 Ruben Valbuena<sup>8</sup>, Bruno Lopes de Faria<sup>19,20</sup>, Celso H. L. Silva Junior<sup>21,22</sup>, Luiz  
12 Aragao<sup>21</sup>, Manuel Eduardo Ferreira<sup>23</sup>, Jingjing Liang<sup>24</sup>, Samuel de Pádua Chaves e  
13 Carvalho<sup>25</sup>, Carine Klauberg Silva<sup>10</sup>

14

15 <sup>1</sup>Department of Forestry, University of Brasília, Campus Darcy Ribeiro, Brasilia, Brazil - 70.910-900;  
16 mairabeatrizteixeira@hotmail.com ; ematricardi@gmail.com

17 <sup>2</sup>School of Forest Resources and Conservation, University of Florida, PO Box 110410 Gainesville, FL  
18 32611, [c.silva@ufl.edu](mailto:c.silva@ufl.edu)

19 <sup>3</sup>Department of Geographical Sciences, University of Maryland, College Park, MD 20740, USA

20 <sup>4</sup>Spatial Ecology and Conservation (SPEC) Lab, School of Forest Resources and Conservation,  
21 University of Florida, Gainesville, FL 32611 USA [eben@ufl.edu](mailto:eben@ufl.edu)

22 <sup>5</sup>Department of Forest Engineering, Federal University of Viçosa (UFV), Viçosa, MG, Brazil;  
23 [chamaral@ufv.br](mailto:chamaral@ufv.br), [rodrigo.leite@ufv.br](mailto:rodrigo.leite@ufv.br)

24 <sup>6</sup>Department of Geography, University of California—Berkeley, Berkeley, CA 94709, USA;  
25 [mid\\_mohan@berkeley.edu](mailto:mid_mohan@berkeley.edu)

26 <sup>7</sup>Department of Forest Engineering, College of Agriculture and Veterinary, Santa Catarina State  
27 University (UDESC), Lages, SC, Brazil; [veraldo.liesenberg@udesc.br](mailto:veraldo.liesenberg@udesc.br)

28 <sup>8</sup>School of Natural Sciences, Bangor University, Bangor LL57 2W, UK, [jzs19xhz@bangor.ac.uk](mailto:jzs19xhz@bangor.ac.uk)

29 <sup>9</sup>Department of Forest Sciences, “Luiz de Queiroz” College of Agriculture, University of São Paulo  
30 (USP/ESALQ), Piracicaba, SP, Brazil; [danieloraa@usp.br](mailto:danieloraa@usp.br)

31 <sup>10</sup>Federal University of São João Del Rei – UFSJ, Sete Lagoas, MG, Brazil - 35701-970;  
32 [carine\\_klauberg@hotmail.com](mailto:carine_klauberg@hotmail.com); [annelsilva11@gmail.com](mailto:annelsilva11@gmail.com), [lucasgoya42.lr@gmail.com](mailto:lucasgoya42.lr@gmail.com),  
33 [victorcordeiro.ufsj@gmail.com](mailto:victorcordeiro.ufsj@gmail.com), [gustavomarcatti@ufsj.edu.br](mailto:gustavomarcatti@ufsj.edu.br), [hirsch\\_andre@ufsj.edu.br](mailto:hirsch_andre@ufsj.edu.br)

34 <sup>11</sup>Department of Forest Engineering, Federal University of Paraná (UFPR), Curitiba, PR, Brazil;  
35 [anacorte@ufpr.br](mailto:anacorte@ufpr.br), [francielrexx@gmail.com](mailto:francielrexx@gmail.com)

36 <sup>12</sup>Technosylva Inc, La Jolla, CA, USA, [adriancardil@gmail.com](mailto:adriancardil@gmail.com)

37 <sup>13</sup>Department of Crop and Forest Sciences, University of Lleida, Lleida, Spain

38 <sup>14</sup>Joint Research Unit CTFC - AGROTECNIO, Solsona, Spain

39 <sup>15</sup>Departamento de Silvicultura, Universidade Federal Rural do Rio de Janeiro, Rua da Floresta,  
40 Seropédica, RJ, 23897-005, Brazil; [brunomendonca@ufrj.br](mailto:brunomendonca@ufrj.br)

41 <sup>16</sup>Federal Institute of Education, Science and Technology of São Paulo, SP, 11533-160, Brazil;  
42 [hamamura.caio@ifsp.edu.br](mailto:hamamura.caio@ifsp.edu.br)

43 <sup>17</sup>US Department of Agriculture, Forest Service, Rocky Mountain Research Station, 1221 South Main  
44 Street, Moscow, ID 83843, USA, [andrew.hudak@usda.gov](mailto:andrew.hudak@usda.gov)

45 <sup>18</sup>Spatial Ecology and Conservation (SPEC) Lab, Center for Latin American Studies, University of  
46 Florida, Gainesville, FL 32611 USA [aalmeyda@ufl.edu](mailto:aalmeyda@ufl.edu)

47 <sup>19</sup>Federal Institute of Technology North of Minas Gerais (IFNMG), 39100-000, Diamantina, MG,  
48 Brazil

49 <sup>20</sup>Department of Forest Science, Federal University of Vales do Jequitinhonha e Mucuri, (UFVJM)  
50 Campus JK, Diamantina, MG, Brazil, [blfaria@gmail.com](mailto:blfaria@gmail.com)

51 <sup>21</sup>National Institute for Space Research (INPE), Earth Observation and Geoinformatics Division, Av.  
52 dos Astronautas, 1758, São José dos Campos SP 12227-010, Brazil, [celsohlsj@gmail.com](mailto:celsohlsj@gmail.com),  
53 [luiz.aragao@inpe.br](mailto:luiz.aragao@inpe.br)

54 <sup>22</sup>Image Processing and GIS Lab (LAPIG), Universidade Federal de Goiás, 74001-970, Goiânia-GO,  
55 Brazil, [mferreira.geo@gmail.com](mailto:mferreira.geo@gmail.com)

56 <sup>23</sup>Universidade Estadual do Maranhão (UEMA), Departamento de Engenharia Agrícola, São Luís,  
57 MA, 65055-310, Brazil

58 <sup>24</sup>Department of Forestry and Natural Resources, Purdue University, West Lafayette, IN, USA,  
59 [alpenbering@gmail.com](mailto:alpenbering@gmail.com)

60 <sup>25</sup>College of Forestry, Federal University of Mato Grosso, Av. Fernando Correa da Costa, 2367, Boa  
61 Esperança, Cuiabá, MT 78060-900, Brazil, [sam.padua@gmail.com](mailto:sam.padua@gmail.com)

62 \*Corresponding author: Tel: + 55 (64) 9653-3427; Email: [mairabeatrizteixeira@hotmail.com](mailto:mairabeatrizteixeira@hotmail.com)

63

64 **Abstract:** Tropical savanna ecosystems play a major role in the seasonality of the  
65 global carbon cycle. However, their ability to store and sequester carbon is uncertain  
66 due to combined and intermingling effects of anthropogenic activities and climate  
67 change, which impact wildfire regimes and vegetation dynamics. Accurate  
68 measurements of tropical savanna vegetation aboveground biomass (AGB) over broad  
69 spatial scales are crucial to achieve effective carbon emission mitigation strategies.  
70 UAV-lidar is a new remote sensing technology that can enable rapid 3-D mapping of  
71 structure and related AGB in tropical savanna ecosystems. This study aimed to assess  
72 the capability of high-density UAV-lidar to estimate and map total (tree, shrubs, and  
73 surface layers) aboveground biomass density (AGBt) in the Brazilian Savanna  
74 (Cerrado). Five ordinary least square regression models estimating AGBt were  
75 adjusted using 50 field sample plots (30m x 30 m). The best model was selected under  
76 Akaike Information Criterion, adjusted coefficient of determination ( $adj.R^2$ ), absolute  
77 and relative root mean square error (RMSE), and used to map AGBt from UAV-lidar  
78 data collected over 1,854 ha spanning the three major vegetation formations (forest,  
79 savanna, and grassland) in Cerrado. The model using vegetation height and cover was  
80 the most effective, with an overall model  $adj.R^2$  of 0.79 and a leave-one-out cross-  
81 validated RMSE of 19.11 Mg/ha (33.40%). The uncertainty and errors of our  
82 estimations were assessed for each vegetation formation separately, resulting in  
83 RMSEs of 27.08 Mg/ha (25.99%) for forests, 17.76 Mg/ha (43.96%) for savannas, and  
84 7.72 Mg/ha (44.92%) for grasslands. These results prove the feasibility and potential of  
85 the UAV-lidar technology in Cerrado but also emphasize the need for further  
86 developing the estimation of biomass in grasslands, of high importance in the  
87 characterization of the global carbon balance and for supporting integrated fire  
88 management activities in tropical savanna ecosystems. Our results serve as a  
89 benchmark for future studies aiming to generate accurate biomass maps and provide  
90 baseline data for efficient management of fire and predicted climate change impacts  
91 on tropical savanna ecosystems.

92

93 **Keywords:** biomass, vegetation, tropical savanna, remote sensing, Cerrado,  
94 mapping, GatorEye

## 95 **1. Introduction**

96 Tropical savanna ecosystems occupy approximately 20% of the Earth's  
97 terrestrial surface and are recognized globally for their species richness and  
98 endemic biodiversity (Simon et al., 2009). These ecosystems are characterized by a  
99 gradient of vegetation formations ranging from grasslands to savannas to forests.  
100 Wildfires are an important element of the tropical savanna, but natural fire  
101 regimes have been altered by anthropogenic activities and climate change (Pivello,  
102 2011; Reichstein et al., 2013). Tropical savannas play a major role in the global  
103 carbon budget (Poulter et al., 2014), but their ability to store and sequester carbon,  
104 and the combined impacts of their fire regimes and vegetation dynamics on the  
105 global carbon balance, are still largely unknown (van der Werf et al., 2010; Pugh et  
106 al. 2019; Duvert et al., 2020; Lasslop et al., 2020).

107 The Brazilian Savanna, known as Cerrado, is the second-largest habitat  
108 type in South America, after the Amazon biome, spanning two million km<sup>2</sup> (23.3%  
109 of the Brazilian territory) (Silva and Bates, 2002; Bonanomi et al., 2019). Cerrado is  
110 considered a hotspot for biodiversity and plays an important role in mitigating  
111 climate change and global warming by storing carbon in biomass (Ribeiro et al.,  
112 2011). However, Cerrado is severely threatened by increased anthropogenic  
113 activities and human-driven changes in fire regime (Durigan and Ratter, 2016).  
114 Between 2002 and 2010, the 545,000 km<sup>2</sup> area burned in the Cerrado biome  
115 represented approximately 73% of the total burned area in Brazil (Araújo et al.,  
116 2012), while constituting only 6.4% of the land area. Hence, fire strongly shapes the  
117 vegetation and ecotones in savannas (Hirota et al. 2011; Staver et al. 2011). By  
118 changing vegetation structure, fires also can induce cascading effects that alter  
119 habitat quality for fauna (Lindenmayer et al., 2008).

120 Almost half of the Cerrado's original vegetation has been lost in the last few  
121 decades (Souza et al., 2020), and the remaining areas face continuous

122 environmental threats as a result of the expansion of agricultural production to  
123 supply the increasing global food demand. Innovative monitoring strategies for  
124 understanding the landscape configuration of biomass stocks and their changes  
125 are needed in the Cerrado to develop accurate predictive vegetation dynamics and  
126 climate models that could support decisions and inform policymakers to define  
127 strategies of carbon markets and REDD+ initiatives globally. Moreover, these  
128 strategies are crucial to improve forest fire management techniques that could  
129 contribute to maintaining ecological values in tropical savannas (Ribeiro et al.,  
130 2011; Franke et al., 2018; Levick et al., 2018; Durigan et al., 2020). Given the large  
131 latitudinal gradient and the high environmental, structural, and inter and  
132 intraspecies variability within the Cerrado biome, data collection requires time and  
133 labor-intensive fieldworks (Ottmar et al., 2001; Gwenzi and Lefsky, 2016; Roitman  
134 et al., 2018). Although field data provide the most accurate and straightforward  
135 estimates, field data collections are constrained by time, financial cost, and labor,  
136 making them impractical and expensive to apply for large-scale and/or recurrent  
137 studies (Mohan et al., 2017; Goldbergs et al., 2018; Silva et al., 2020). Additionally,  
138 direct biomass estimation requires destructive sampling that causes some impacts  
139 on local habitat and the ecosystem. Integration of mathematical models and  
140 indirect measurements using remotely sensed data provide complementary or  
141 alternative approaches to estimate biomass and other physical variables (Qureshi  
142 et al., 2012; Ribeiro et al., 2017).

143 Among the remote sensing technologies available, light detection and  
144 ranging (lidar) has gained prominence in recent decades due to its ability to  
145 provide detailed and accurate characterizations of vertical vegetation structure in  
146 tropical savanna ecosystems (Gwenzi and Lefsky, 2016; Levick et al., 2018;  
147 Goldbergs et al., 2018; Zimbres et al., 2020). These three-dimensional structural  
148 assessments can be undertaken by spaceborne (SLS), airborne (ALS), or terrestrial  
149 laser scanning (TLS) platforms, although the latter is constrained by limited spatial

150 footprints and thus is not directly applicable for broad-scale studies (Ferreira et al.,  
151 2012; Ribeiro et al., 2017; Silva et al., 2018; Luck et al., 2020; Valbuena et al., 2020;  
152 Zimbres et al., 2020; Singh et al., 2021). The advent of unmanned aerial vehicles  
153 (UAVs) has further expanded the capabilities of airborne lidar, as UAV-lidar is an  
154 easily implementable and cost-effective solution that bridges the scale gap between  
155 ALS and TLS collections and improves the accuracy of outputs such as tree height,  
156 leaf area density, and biomass (Wang et al., 2019; Almeida et al., 2020; Dalla Corte  
157 et al., 2020; Harkel et al., 2020; Shendryk et al., 2020).

158         Notwithstanding the demonstrated potential of lidar in estimating biomass  
159 at both landscape and regional scales by previous studies (Drake et al., 2002;  
160 Naasset and Gobakken, 2008; Hudak et al., 2020), they are still rarely implemented  
161 in tropical savanna. Additionally, the majority of the undertaken studies have  
162 placed their primary focus solely on the estimation of biomass from trees, using  
163 ALS and TLS (e.g., Bispo et al. 2020; Zimbres et al., 2020), or the recent SLS  
164 missions, such as NASA Global Ecosystem Dynamics Investigation (GEDI)  
165 (Dubayah et al. 2020; Marselis et al. 2019; Marselis et al. 2020). The very few studies  
166 that have ventured into estimating individual biomass components have limited  
167 their purview with the assessment of biomass contributions from tree strata, such  
168 as leaves, branches, and stems (García et al. 2010; Silva et al. 2014; Hernando et al.  
169 2017; Scaranello et al. 2019). However, a significant portion of the total  
170 aboveground biomass in tropical savanna is composed of surface biomass (duff,  
171 litter, downed woody debris, shrub, and herbaceous), which are not taken into  
172 account by the foregoing studies. These, however, have great influence on fire  
173 regimes and associated carbon cycles (Pivello, 2011). Therefore, it is crucial to fill in  
174 the gap between global carbon fluxes and current remote sensing estimations of  
175 biomass in terrestrial ecosystems, with the development of models that account for  
176 large components of ecosystem biomass that remain unaccounted for when only  
177 woody tree biomass is considered (Dass et al., 2018).

178 Even though lidar has been shown to be beneficial for capturing the 3-D  
179 structures of the vegetation in savanna ecosystems ([Anderson et al., 2018](#); [Bispo et](#)  
180 [al. 2020](#); [Zimbres et al., 2020](#)), there is a need to develop a framework for mapping  
181 total (woody, shrubs and surface vegetation) total aboveground biomass density  
182 (AGBt) and evaluate the applicability of UAV-lidar for AGBt in tropical savanna  
183 ecosystems. This study aimed to assess the capability of high-density UAV-lidar to  
184 estimate and map AGBt across the structurally complex vegetation formations of  
185 the Cerrado in Brazil. Herein, we developed a framework for: (i) selecting the best  
186 UAV-lidar metrics to build AGBt models; (ii) shortlisting the best models to  
187 predict AGBt; (iii) estimating AGBt at plot level; and (iv) mapping AGBt at the  
188 landscape level, assessing its spatial distribution and uncertainty across the main  
189 Cerrado vegetation formations: grassland, savanna, and forest. Given the resource-  
190 grade accuracy available through high-density UAV-lidar ([Wilkinson et al., 2019](#)),  
191 we hypothesize that it would be possible to map AGBt in Cerrado at a satisfactory  
192 precision, and we expect to identify biome-specific technological challenges that  
193 need to be addressed for furthering our understanding of the existing ecosystem  
194 intricacies and advancement of carbon management paradigms. Since there exist  
195 no other UAV lidar-based studies on total AGB density estimates for the Cerrado  
196 biome, this work is intended to serve as a benchmark for future studies and should  
197 help generate consistent AGBt maps even as the climate and environment are  
198 changing.

199

## 200 **2. Material and Methods**

### 201 **2.1. Study area**

202 Our study sites are located at the Serra do Cipó National Park (SCNPK),  
203 Chapada dos Veadeiros National Park (CVNPK), Paraopeba National Forest  
204 (PNF), and University of São João Del-Rei's Forest (UFSJ) (Fig. 1).

205 SCNPK (19°12'-34'S, 43°27'-38'W) is located in the southeast portion of the  
206 Cerrado biome, state of Minas Gerais. The region's climate is mesothermal, Cwb  
207 (subtropical of altitude) according to Koppen's classification (Alvares et al., 2013),  
208 with dry winters and rainy summers, and annual rainfall averages ca. 1,400 mm,  
209 with a rainy season occurring between October and March, and monthly rainfall  
210 ranging from 75 to 340 mm (Alvarado et al., 2017). The average annual  
211 temperature ranges from 17.0° to 18.5°C. The study site's topography is rugged  
212 and predominantly mountainous, with elevations ranging from 750 to 1,670 m  
213 above sea level (a.s.l.) (Ribeiro and Figueira, 2017). The vegetation in SCNPK  
214 varies and comprises different physiognomies, from open grasslands ("Campo  
215 Limpo") at altitudes below 1,000 m to savanna formations with different  
216 proportions of woody cover ("Campo Sujo", "Campo Cerrado" and "Cerrado  
217 sensu stricto") and forest formations ("Cerradão"), all classified as part of the  
218 Cerrado sensu lato (Oliveira-Filho and Ratter, 2002); above 1,000 m are found the  
219 rupestrian grasslands (Benites et al., 2003). The soils are diverse and vary  
220 according to the vegetation formations, being greatly determined by microclimatic  
221 gradients associated with local topography. In savanna and forest formations,  
222 there are latosols and cambisols, while in the rupestrian grasslands there are  
223 litholic neosols and spodosols (Schaefer et al., 2016).

224 The CVNPK (13°51'-14°10'S, 47°25'-42'W) encompasses five municipalities  
225 in the state of Goiás, Brazil. Within a mountainous region, the altitude in CVNPK  
226 ranges from 620 to 1,700 m a.s.l., and the climate is characterized as tropical and  
227 sub-humid (AW) (Alvares et al., 2013). The average temperatures range from 20° to  
228 26°C (Silva et al., 2001). The landscape is formed by mosaics of different vegetation  
229 types (Ribeiro and Walter, 2008) characterized by a predominance of savannas at  
230 high elevations and forest formation at low elevations (Felfili et al. 2007). Dry and  
231 wet grasslands and savannas cover most of the landscape and occur in between  
232 streams. Dry deciduous forests are found at the northwest edge of the park,

233 whereas riparian evergreen forests are most common at the southwest edge of the  
234 park (Flores et al., 2020). In total, the CVNPK comprises 77% of savanna formation,  
235 and about 10% corresponds to the forest fragments (Porto et al., 2011). Cambisols  
236 and litholic neosols occupy the largest area of the park (IBAMA, 1998).

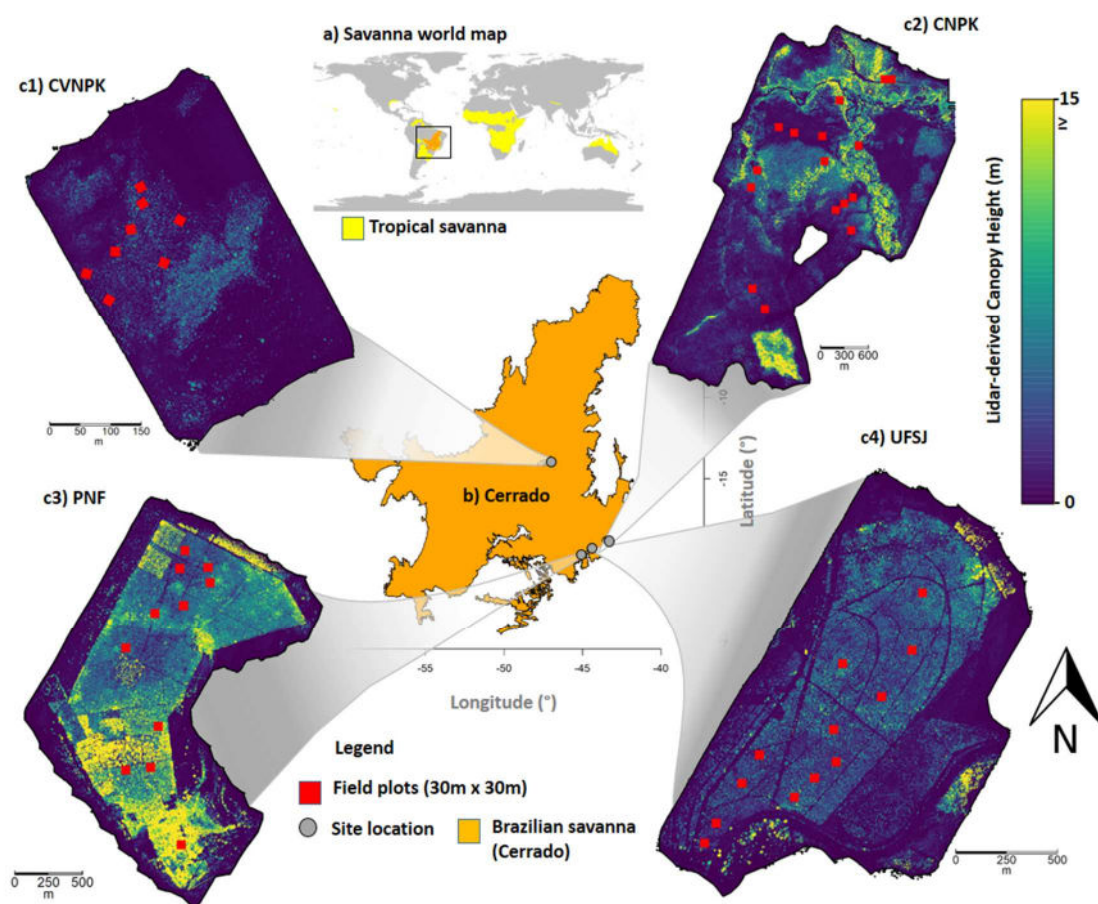
237         The PNF (19° 20'S and 44° 20'W) is located in the municipality of Paraopeba,  
238 state of Minas Gerais, Brazil. It is comprised of 150 ha remnants of Cerrado  
239 vegetation, including both savanna (e.g., Cerrado *sensu stricto*) and forest  
240 formations (e.g.Cerradão) (Neri et al., 2013). The altitude in PNF ranges from 734  
241 to 750 m a.s.l., and the climate is characterized by the humid subtropical type (Cfa)  
242 (Alvares et al. 2013), with a rainy summer from January to March and a dry season  
243 that occurs from April to September, with a mean annual precipitation of 1,236  
244 mm (Balduino et al. 2005). The soils range from Latosols (red, red-yellow, and  
245 yellow) to cambisols and fluvic neosols (Neri et al., 2013).

246         The UFSJ forest (19°28'S, 44°11'W) is located in the Sete Lagoas  
247 municipality, state of Minas Gerais, Brazil, at an altitude that ranges from 742 to  
248 815 m. The local climate is considered tropical altitude (Cwa) (Alvares et al., 2013),  
249 with a well-defined dry winter and rainy summer. The average annual  
250 temperature is 21.73°C, and the mean annual precipitation is 1,330 mm (Guimarães  
251 and Rios, 2010). The predominant vegetation type is Cerrado *sensu stricto*  
252 characterized by the dominance of trees with scattered shrubs and grass  
253 understorey. The climate is of the humid subtropical type, with a dry winter and  
254 moderately hot summer (Alvares et al., 2013). The soils are predominantly Oxisols  
255 (red latosol and red-yellow latosols).

256         Altogether, our four study sites represent various Cerrado vegetation  
257 physiognomies spanning a wide range in vertical and horizontal vegetation  
258 structures, and also in species diversity and provenances. Herein, we classified the  
259 vegetation of our study sites into three major formations according to Ribeiro and  
260 Walter (2008) and defined as: (i) grasslands, mostly represented by a shrub-

261 herbaceous layer with absence or randomly sparse taller shrub individuals; (ii)  
262 savannas, which feature a continuous shrub-herbaceous layer and a discontinuous  
263 tree layer that ranges in density and never closes completely; and (iii) forests,  
264 mostly represented by a continuous tree layer but also very structurally diverse as  
265 a result of the species communities partitioning under different environmental  
266 conditions. (Fig. 2).

267



268

269 **Figure 1.** Map of the UAV-lidar-derived vegetation height within the study area in  
270 the Brazilian Cerrado. Serra do Cipó National Park (SCNPK), Chapada dos  
271 Veadeiros National Park (CVNPK), Paraopeba National Forest (PNF), and  
272 University of São João Del-Rei's Forest (UFSJ).

273

274 **2.2. Field measurements**

275 Field plots of 30 m × 30 m (900 m<sup>2</sup>) covering all the Cerrado formations (Fig.  
 276 2) were established between June and July of 2019 for measuring the vegetation  
 277 total aboveground biomass density (AGB<sub>t</sub>). Plot corners were registered using a  
 278 Differential Global Navigation Satellite System (DGNSS). The aboveground  
 279 biomass density of trees (AGB<sub>Trees</sub>, in Mg/ha) was determined from measurements  
 280 of all individual trees within the plot with a diameter at breast height (dbh, in cm)  
 281 ≥ 10 cm. Every tree was taxonomically identified, and their heights (ht, in m) and  
 282 dbh were measured using a clinometer and diameter tape, respectively. Within  
 283 each plot, two 2 m × 5 m sub-plots were established to determine the aboveground  
 284 biomass density of shrubs and small trees (dbh < 10 cm) (AGB<sub>ST</sub>, in Mg/ha). For  
 285 each plot, four 1 m × 1 m sub-plots were established for determining the  
 286 aboveground biomass density of surface vegetation (AGB<sub>SB</sub>, in Mg/ha). The AGB<sub>t</sub>  
 287 was calculated as the sum of the biomass density (in Mg/ha) components  
 288 measured within each plot and sub-plots, each component having been  
 289 transformed into biomass density (in Mg/ha) using their corresponding hectare  
 290 expansion factors (HEF).

291 Individual tree dry biomass was estimated in the field using a published  
 292 allometry equation calibrated (Eq. 1) based on dbh, ht and wood density ( $\rho$ )  
 293 information (Chave et al 2014). Total dry tree biomass density (AGB<sub>ST</sub>, in Mg/ha)  
 294 was computed by summing up individual tree biomass to the plot level (Eq. 2):

$$AGB_{Tree_i} = 0.0673 * (\rho \times dbh^2 * ht_i)^{0.976} \quad (\text{Eq.1})$$

$$AGB_{Trees} = \sum_{i=1}^n AGB_{tree_i} * HEF_{Trees} \quad (\text{Eq. 2})$$

296 where: dbh is in cm, ht is in m, and  $\rho$  is in g.cm<sup>-3</sup>. AGB<sub>Trees</sub> represents the total dry  
 297 tree biomass density at the plot level, AGB<sub>Tree\_i</sub> represents dry biomass (in kg) per

298 tree  $i$ , and  $n$  represents the number of trees for each plot  $i$ , and  $HEF_{Trees} = 11.11$ .  
299 Wood density values  $\rho$  were derived from [Zanne et al. \(2009\)](#).

300 For measuring the AGB stock in the 2 m  $\times$  5 m shrub sub-plots, we  
301 harvested all the shrubs and small trees and weighed them using a 10 g precision  
302 scale. Three  $\sim$ 500 g samples per sub-plot containing both the shrub and tree  
303 components (stems, branches, and leaves) were sent to the laboratory to measure  
304 the weights of wet biomass (WB, in g) and dry biomass (DB, in g) biomass.  
305 Average WB and DB values were used to calculate moisture content ( $MC_i$ , in %)  
306 for each sub-plot, according to Eq. 3. Total dry shrub and small tree biomass  
307 density ( $AGB_{ST}$ , in Mg/ha) was then calculated as:

$$MC_i = \frac{WB_i - DB_i}{WB_i} \quad (\text{Eq. 3})$$

$$AGB_{ST} = \sum_{i=1}^n AGB_{ST_i} * HEF_{ST} * (1 - MC_i) \quad (\text{Eq. 4})$$

308 where  $AGB_{ST}$  is the dry shrub and small tree biomass density at the plot level,  
309  $AGB_{ST_i}$  is the wet shrub and small tree biomass for sub-plot  $i$  (in kg),  $MC_i$  is the  
310 moisture content calculated for each sub-plot, and  $HEF_{ST} = 500$ .

311 For computing the surface vegetation biomass at the plot level, in the field,  
312 we collected and weighed the biomass of duff, litter, downed woody material, and  
313 herbaceous material found within the 1 m  $\times$  1 m sub-plots. Again, three  $\sim$ 500 g  
314 samples per sub-plot were also collected and sent to the laboratory for computing  
315 the  $MC_i$  for the surface biomass (Eq. 3). The total dry surface biomass density  
316 ( $AGB_{SB}$ , in Mg/ha) was then calculated as:

317

$$AGB_{SB} = \sum_{i=1}^n AGB_{SB_i} * HEF_{SB} * (1 - MC_i) \quad (\text{Eq. 5})$$

318 where  $AGB_{SB}$  is the dry surface biomass density at the plot level, and  $AGB_{SBi}$  is the  
 319 wet surface biomass for sub-plot  $i$  (in kg),  $MC_i$  is the moisture content calculated  
 320 for each sub-plot, and  $HEF_{SB} = 2,500$ .

321

322 Finally, the total dry aboveground biomass density ( $AGB_t$ , in Mg/ha) at the  
 323 plot level was then computed by summing the  $AGB_{tree}$ ,  $AGB_{ST}$ , and  $AGB_{SB}$   
 324 measurements (Eq. 6).

325

$$AGB_t = AGB_{Trees} + AGB_{ST} + AGB_{SB} \quad (\text{Eq. 6})$$

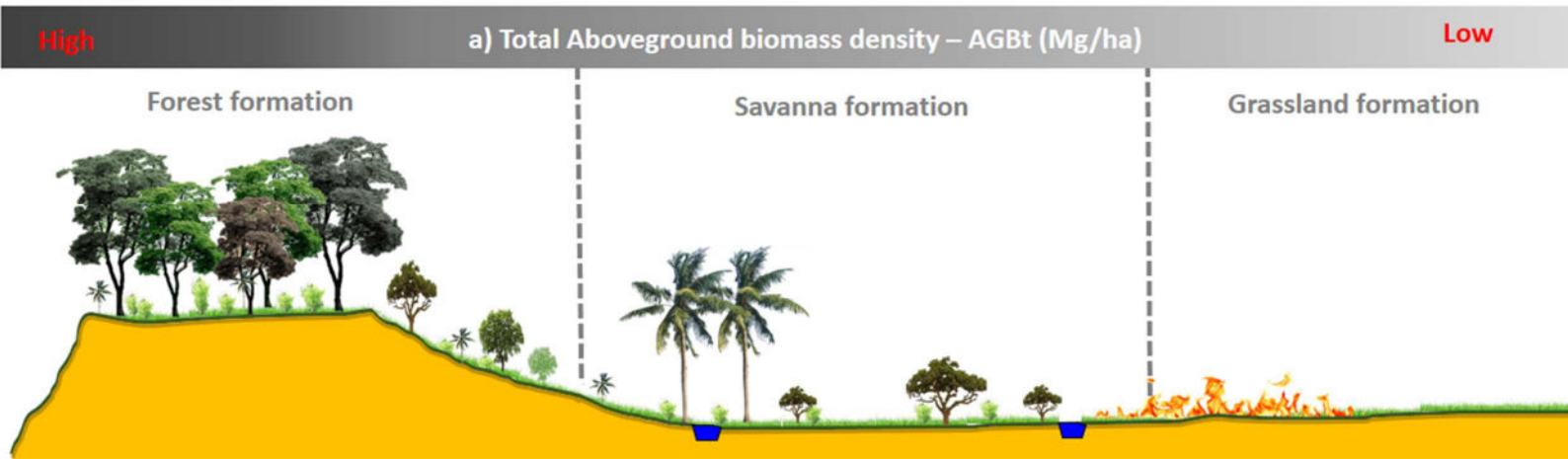
326 The summary of  $AGB_t$  within all the field plots and stratified by Cerrado  
 327 formations is presented in Table 1.

328

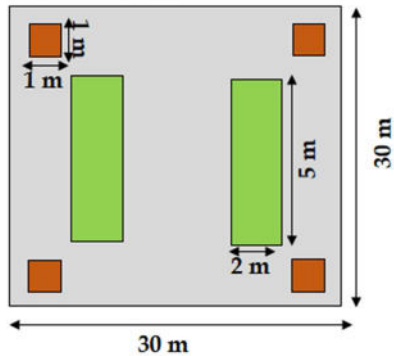
329 **Table 1.** Summary of the total aboveground biomass density ( $AGB_t$ ) within our  
 330 field plots and stratified by Cerrado formations.

| Formation | Number<br>of plots | AGBt (Mg/ha) |        |        |       |
|-----------|--------------------|--------------|--------|--------|-------|
|           |                    | min          | max    | mean   | sd    |
| Grassland | 5                  | 11.65        | 25.86  | 17.19  | 7.30  |
| Savanna   | 30                 | 13.32        | 100.22 | 40.39  | 23.55 |
| Forest    | 15                 | 43.68        | 187.94 | 104.21 | 42.39 |

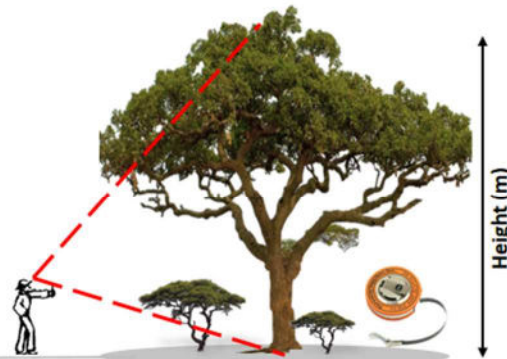
a) Vegetation formations



b) Plot design



c) Tree ht and dbh measurements



d) Surface biomass measurement



Biomass components measured:

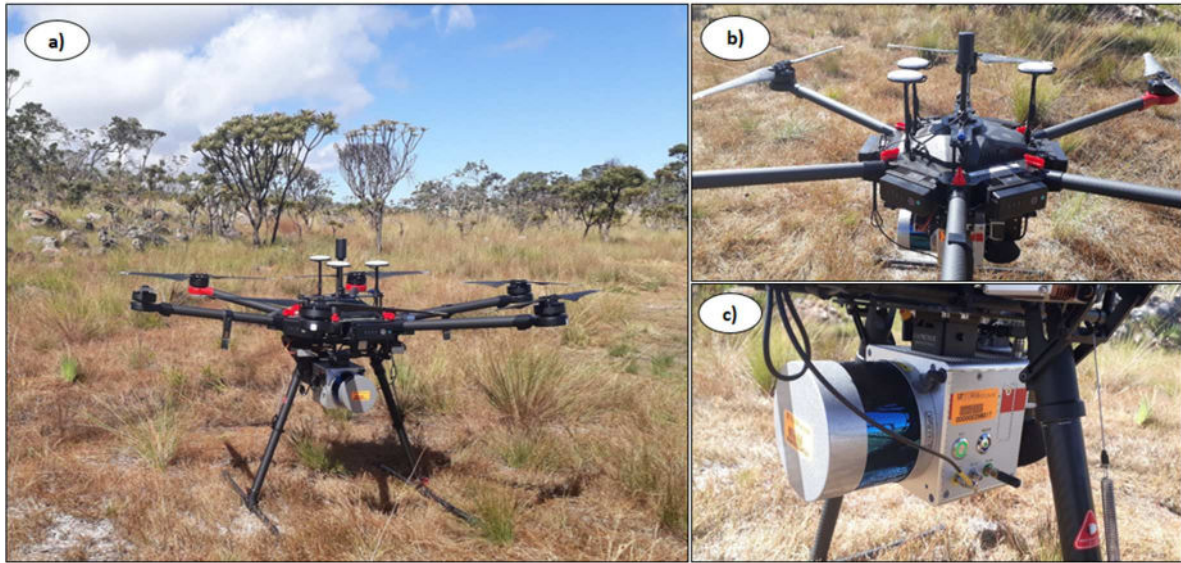
- Trees (dbh  $\geq$  10 cm)
- Shrubs and trees (dbh < 10 cm)
- Surface (duff, litter, downed woody and herbaceous)

331

332 **Figure 2.** Illustration of field data collection. a) Cerrado formation, b) design of field plots and subplots for measuring the total  
 333 aboveground biomass (AGBt), and c) Tree dbh and height measurements, d) surface biomass measurement.

### 334 2.3. UAV-lidar

335 Our study sites were scanned using the GatorEye UAV-lidar system (Fig. 3)  
336 (Almeida et al., 2020; Prata et al., 2020; Dalla Corte et al., 2020) during two weeks  
337 in July 2019, which was nearly simultaneous with the field data collection. The  
338 GatorEye uses a DJI M600 Pro platform mounted with a Phoenix Scout Ultra core  
339 to integrate lidar with an inertial motion unit (Novatel STIM 300), and cm accuracy  
340 differential GNSS system, which have a combined weight of approximately 4.5 kg.  
341 The lidar sensor, which was uniquely used in this study, was a Velodyne VLP-32c  
342 dual-return laser scanner which has a total of 32 separate lasers each having a 360°  
343 vertical field of view (FOV) and which are distributed to permit an instantaneous  
344 40° along-track FOV. The laser suite emits 600,000 pulses per second and a  
345 theoretical return number of 1,200,000 per second, which during flight with an  
346 across-track FOV of 120° creates a realized approximate 350,000 returns per  
347 second, with the remaining going out of range. A ground base station X900S-OPUS  
348 GNSS receiver collected static GNSS data, which were used to calculate a PPK  
349 (post-processed kinematic) flight trajectory using Novatel Inertial Explorer  
350 software. Absolute point accuracy was tested using ground-surveyed DGNSS  
351 checkpoints, and it was accepted when showing a root mean square error (RMSE;  
352 eq. 10) below 5 cm (Wilkinson et al., 2019). Detailed information and data  
353 downloads can be found at the GatorEye website ([www.gatoreye.org](http://www.gatoreye.org)) (Broadbent  
354 et al., 2020) and in d'Oliveira et al. (2020). The autonomous flight was programmed  
355 to survey at a mean speed of 14 m/s at around 100 m above ground level (a.g.l.),  
356 with flightlines spaced 100 m apart. In total, across the four study sites, we flew  
357 approximately 600 km of flight lines covering 1,854 hectares, which to our  
358 knowledge is the largest area of UAV-lidar used in a publication (as of 12/16/20).  
359 The final merged point clouds were about 100 GB in total size and had a very high-  
360 density of approximately 450 points/m<sup>2</sup> across all study sites.



361  
 362 **Figure 3.** GatorEye UAV-lidar system. a) GatorEye UFL (Gen 1) system, with  
 363 Phoenix Scout Ultra, hyperspectral, and visual sensors on a DJI M600 Pro airframe;  
 364 b) GNSS antennas for navigation (three) and sensor trajectory (middle); and c)  
 365 Velodyne Ultra Puck (lidar system).

366

367         The UAV-lidar 3-D point cloud data was processed using the GatorEye  
 368 Multi-scalar Post-Processing Workflow, followed by further flight line alignment  
 369 using Bayes StripAlign software, as it is described in detail in [Broadbent et al.](#)  
 370 [\(2020\)](#). The final elliptical merged point clouds were further processed using  
 371 Lastools ([Isenburg, 2020](#)). First, the las files were divided into tiles of 200 m for  
 372 ground return classification via *lasground* (spike: 1 m, bulge: 0.5 m, step: 10 m,  
 373 offset: 0.05 m). Digital terrain models (DTM) were created with a spatial resolution  
 374 of 1 m via the *blast2dem* and used for normalizing the 3-D point cloud to height  
 375 a.g.l. via *lasheight*. The *Lasclip* tool was used for clipping the point cloud within the  
 376 field plots, and the *lascanopy* tool was applied for computing a suite of lidar canopy  
 377 height and cover metrics per plot and for the entire lidar coverage as grid layers  
 378 with a spatial resolution of 30 m (see Table 2).

379

380

381

**Table 2.** UAV-lidar derived metrics.

| Class  | Metrics                | Description                                     |
|--------|------------------------|---|
| Height | HMEAN                  | Height mean                                     |
|        | HMAX                   | Height maximum                                  |
|        | HSD                    | Height standard deviation                       |
|        | HKUR                   | Height kurtosis                                 |
|        | HSKE                   | Height skewness                                 |
|        | HOME                   | Height of Median Energy                         |
|        | H25TH                  | Height 25th percentile                          |
|        | H50TH                  | Height 50th percentile                          |
|        | H70TH                  | Height 70th percentile                          |
|        | H75TH                  | Height 75th percentile                          |
|        | H80TH                  | Height 80th percentile                          |
|        | H85TH                  | Height 85th percentile                          |
|        | H90TH                  | Height 90th percentile                          |
|        | H95TH                  | Height 95th percentile                          |
| H98TH  | Height 98th percentile |   |
| H99TH  | Height 99th percentile |   |
| Cover  | COV                    | Cover (percentage of first return above 1.30 m) |

382

383 **2.4. Modeling development and assessment**

384 Our modeling framework was based on linear regression models (Eq. 7)  
385 fitted using the ordinary least squares (OLS) estimator (Eq. 8). Herein, a family of  
386 five models was developed in two steps by first removing high correlated metrics,  
387 and second selecting the best models using the best subsets of predictors (Hudak  
388 et al., 2006; Silva et al., 2014). First, Pearson’s correlation ( $r$ ) was used to identify  
389 and exclude highly correlated variables using a  $\pm 0.9$  threshold. Subsequently, we  
390 applied an exhaustive variable selection algorithm to find the best linear models  
391 with up to six predictors using the *regsubsets* function of the R package leaps  
392 (Hudak et al., 2006; Lumley, 2020). The linear models were fitted using the natural  
393 logarithm transformation of the AGBt as a response and the non-correlated lidar-  
394 derived metrics as predictor variables. The heteroscedasticity and normality of the

395 model residuals were tested with the Breusch-Pagan (Breusch and Pagan, 1979)  
 396 and Shapiro-Wilk (Shapiro and Wilk, 1965) tests at the significance level of 0.05.

$$Y_S = X_S\beta + \varepsilon_S \quad (\text{Eq. 7})$$

397 where:  $Y_S$  is the  $n$ -length column vector of the response variable AGBt in sample  $S$ ;  
 398  $X_S$  is an  $n \times (p + 1)$  matrix of the lidar metrics used as predictors and a unit vector  
 399 as the first column;  $\beta$  is a column vector of model parameters of length  $(p + 1)$ ; and  
 400  $\varepsilon_S$  is the  $n$ -length column vector of random errors with  $E(\varepsilon_S) = 0$  and  $\varepsilon_i \sim N(0, \sigma_\varepsilon^2)$ .  
 401 Using the sample  $S$  of  $n = 50$  plots, the vector of model parameters was estimated  
 402 for each model as:

$$\hat{\beta}_S = (X_S^T X_S)^{-1} X_S^T Y_S \quad (\text{Eq. 8})$$

403 where:  $\hat{\beta}_S$  is a column vector of estimated model intercept and parameters with  
 404 length  $(p + 1)$ , and  $p$  is the number of predictors.

405 We calculated the adjusted coefficient of determination ( $\text{adj}R^2$ ) and the  
 406 absolute and relative root mean square error (RMSE and %RMSE, respectively),  
 407 and absolute and relative mean differences (%MD), between the estimated and  
 408 observed AGBt values (Eqs. 9-13) to assess the models' performance. The models  
 409 were ranked using the corrected Akaike information criterion (AICc, Eq. 14)  
 410 (Sugiura, 1978; Hudak et al., 2006). The AICc can be applied when the number of  
 411 observations is relatively small ( $n/p < 40$ ) and computes an additional penalization  
 412 for the number of parameters to the AIC (Akaike 1979).

$$\text{adj}R^2 = 1 - \frac{(1 - R^2)(n - 1)}{n - p - 1} \quad (\text{Eq. 9})$$

$$\text{RMSE} = \sqrt{\frac{\sum_{i=1}^n (\hat{Y}_i - Y_i)^2}{n}} \quad (\text{Eq. 10})$$

$$\% \text{RMSE} = \frac{\text{RMSE}}{\bar{Y}} * 100 \quad (\text{Eq. 11})$$

$$\text{MD} = \frac{\sum_{i=1}^n (\hat{Y}_i - Y_i)}{n} \quad (\text{Eq. 12})$$

$$\%MD = \frac{MD}{\bar{Y}} * 100 \quad (\text{Eq. 13})$$

$$AICc = AIC + 2p \frac{(p+1)}{(n-p-1)}, \quad (\text{Eq. 14})$$

413 where:  $\hat{Y}_i$  is the estimated AGBt;  $Y_i$  is the observed AGBt;  $\bar{Y}$  is the sample mean  
 414 observed AGBt;  $n$  is the number of observations, and  $p$  is the number of predictors.  
 415 All performance assessments were carried out using the AGBt on its original scale.  
 416 The back-transformation was conducted by applying the inverse natural logarithm  
 417 to the AGBt values. The estimated values were further multiplied by a correction  
 418 factor (Eq. 15) to reduce MD related to the log-transformation (Smith 1993, Hudak  
 419 et al. 2006).

$$cf = e^{(0.5 \times MSE)} \quad (\text{Eq. 15})$$

420 where: MSE is the mean squared error.

421 The model performances were also estimated for the different Cerrado  
 422 formations (grassland, savanna, and forest). The best-ranked model was further  
 423 assessed with a leave-one-out cross-validation (LOOCV) and  $R^2$ , absolute and  
 424 relative RMSE and MD were also calculated based on the observed and estimated  
 425 AGBt values derived from the LOOCV procedure within each vegetation  
 426 formation. The Wilcoxon–Mann–Whitney rank-sum (W) test (Wilcoxon, 1945) was  
 427 applied to assess if the estimated and observed AGBt differ at the significance level  
 428 of 0.05.

429

## 430 2.5. Aboveground biomass mapping

431 The best linear model was implemented across the entire landscape, to map  
 432 the AGBt in the study site. In this step, the lidar-derived metrics used as predictors  
 433 were calculated for a spatially-continuous grid of 30 m × 30 m cells, and the model  
 434 was applied to every grid cell across all the study sites. The Cerrado formations  
 435 were delineated based on visual interpretation of high spatial resolution GatorEye

436 UAV RGB and Planet’s imagery (Planet Team, 2017), conducted by an experienced  
 437 local photo-interpreter.

438 Accounting for the uncertainty of the estimates is important when  
 439 combining inventory and remote sensing data to map forest attributes (Persson  
 440 and Stahl, 2020). We accounted for the uncertainty for each Cerrado formation by  
 441 calculating the variance of the estimator ( $V[\widehat{E}(\mu)_i]$ ) estimated using standard  
 442 model-based inference (Saarela et al. 2016, Stahl et al. 2016, Puliti et al. 2018). In  
 443 this approach, the sample S used to develop the models in section 2.4 was  
 444 considered a draw from a larger population U. The  $U_i$  represents the finite  
 445 population of the  $i$ -th Cerrado formation with  $N_i$  grid-cells. Considering the OLS-  
 446 estimated parameters  $\hat{\beta}_S$  (Eq. 8), the expected mean value ( $\widehat{E}(\mu)_i$ ) and  $V[\widehat{E}(\mu)_i]$  for  
 447 the  $i$ -th Cerrado formation can be estimated with Eq. 16 and Eq. 17.

$$\widehat{E}(\mu)_i = \iota_{U_i}^T X_{U_i} \hat{\beta}_S \quad (\text{Eq. 16})$$

448 where:  $\iota_{U_i}$  is the  $N_i$ -length column vector with values  $1/N_i$  for the  $N_i$  grid cells of  
 449 population  $U_i$  of the  $i$ -th vegetation type;  $X_{U_i}$  is a  $N_i \times (p + 1)$  matrix of the lidar  
 450 metrics used as predictors and a unit vector as the first column.

$$V[\widehat{E}(\mu)_i] = \iota_{U_i}^T X_{U_i} \text{Cov}(\hat{\beta}_S) X_S^T \iota_{U_i} \quad (\text{Eq. 17})$$

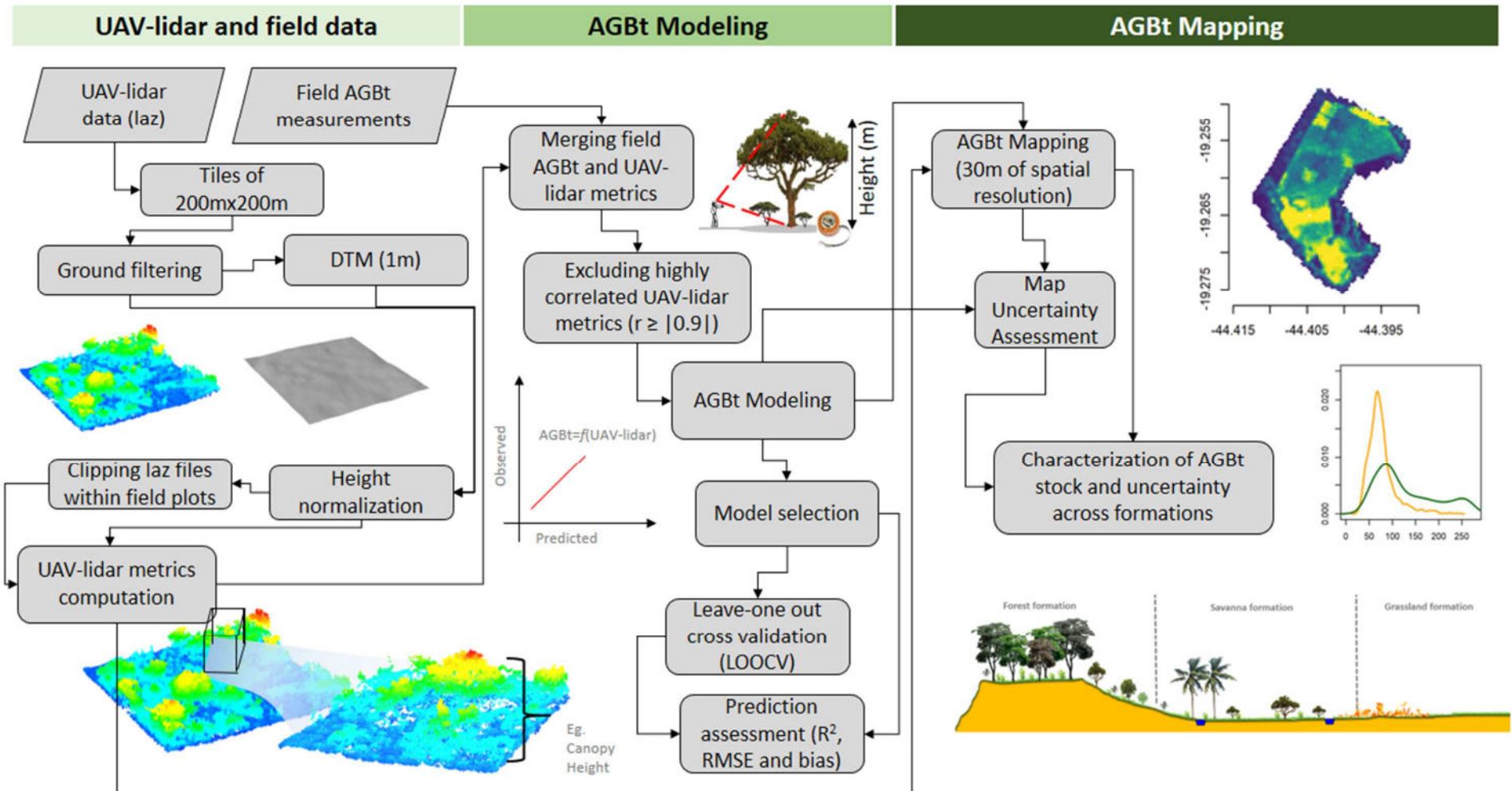
451 where:  $\text{Cov}(\hat{\beta}_S)$  is the covariance matrix of the model parameters  $\hat{\beta}_S$ . Assuming  
 452 that the estimated errors are homoscedastic the  $\text{Cov}(\hat{\beta}_S)$  as calculated by Eq. 18.

$$\text{Cov}(\hat{\beta}_S) = \frac{\hat{\epsilon}_S^T \hat{\epsilon}_S}{n - p - 1} (X_S^T X_S)^{-1} \quad (\text{Eq. 18})$$

453 where:  $\hat{\epsilon}_S$  is the vector of the estimated residuals for the model developed using  
 454 the sample S (Eq. 16). The standard error  $\widehat{SE}_i$  is subsequently then estimated as the

455  $\sqrt{V[\widehat{E}(\mu)_i]}$  and the  $\% \widehat{SE}_i$  as a percentage of the mean estimated AGBt.

456



457  
458

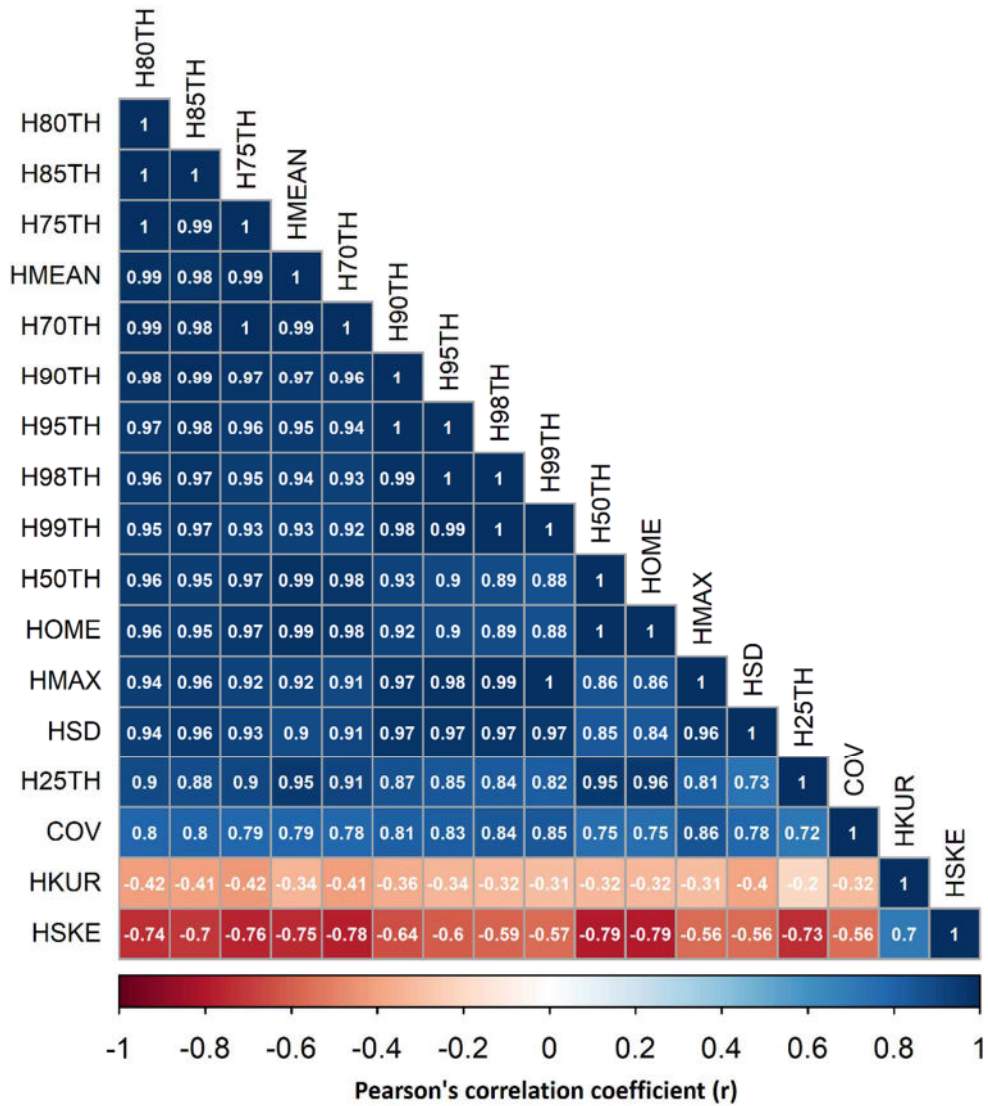
Figure 4. Workflow for the UAV-lidar data processing (left), AGBt modeling (middle), and mapping (right) in Cerrado.

### 459 3. Results

460

#### 461 3.1. UAV-lidar metrics

462 Fig. 5 shows the Pearson's correlation test ( $r$ ) among the 17 UAV lidar-  
463 derived metrics (Table 2). In general, 12 metrics were highly correlated ( $|r| > 0.9$ )  
464 with each other and were therefore excluded from further analysis under the  
465 adopted threshold criteria (Fig. 5). We kept one of the highly correlated metrics  
466 (H98TH), and along with the four remaining metrics (i.e., COV, H50TH, HKUR,  
467 and HSKE), we built the prospective models to estimate AGBt. Three variables  
468 were positively correlated, such as H98TH, COV, and H50TH, while two others  
469 were negatively correlated, such as HKUR, and HSKE (Fig. 4). Although the  
470 number of metrics was reduced to five, the above mentioned lidar-derived metrics  
471 still represented important attributes of the vegetation, such as the dominant  
472 height (e.g., H98TH), the canopy coverage (e.g., COV), and the vegetation's height  
473 asymmetry (e.g., HSKE).



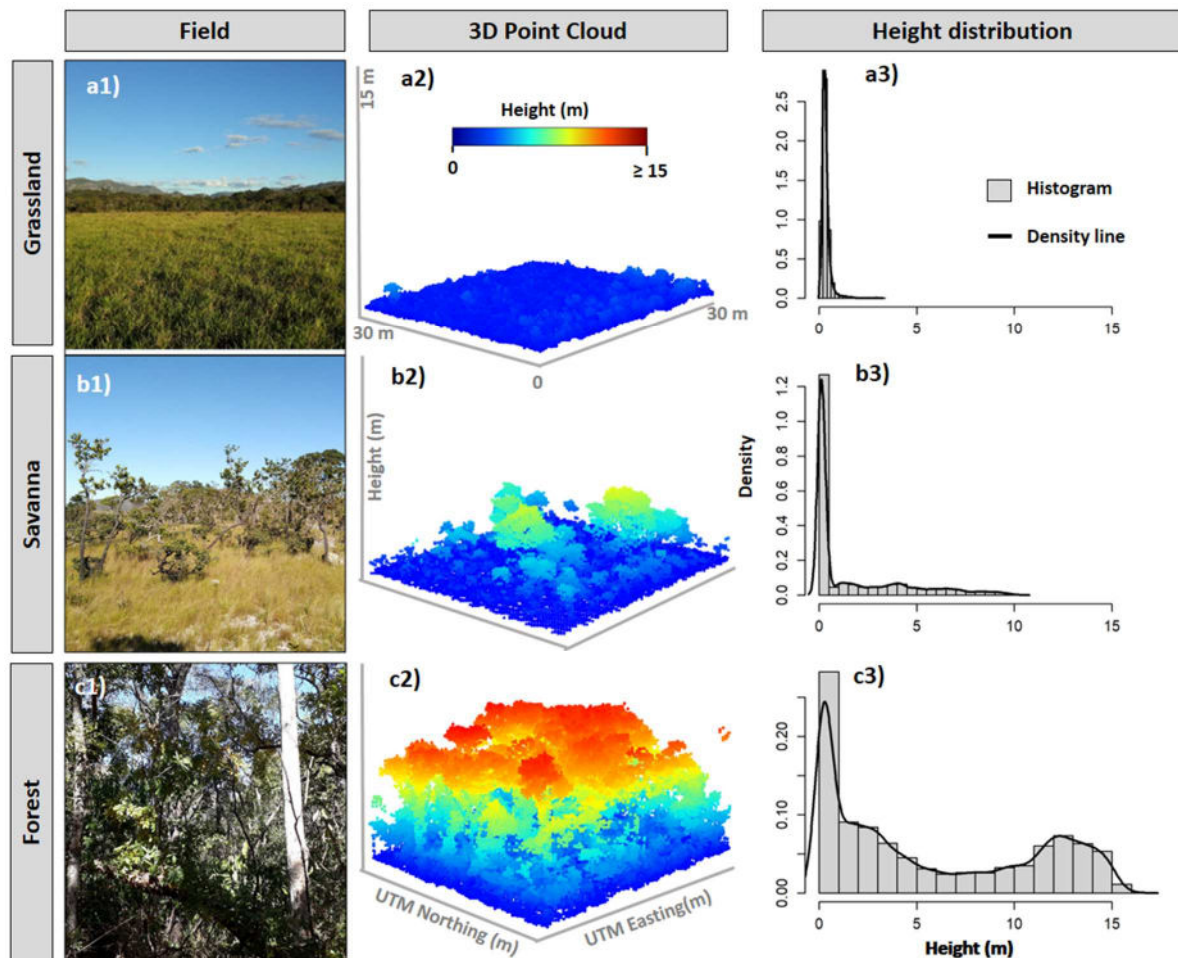
474

475 **Figure 5.** Pearson's correlation (r) diagram among the 17 candidate UAV-lidar  
 476 metrics using a  $|r| > 0.9$  threshold. The values are ranked using a color gradient  
 477 from -1 to 1, where 0 means no correlation and 1 a strong correlation. The negative  
 478 and positive signs indicate inverse and direct relationships between two variables,  
 479 respectively.

480

481 In grasslands, the lidar returns were more concentrated near the ground  
 482 (Fig. 6.a1-a3) because of the lower vegetation structure and variability found in  
 483 this formation. This is clearly illustrated by inspecting the 3-D view perspective of  
 484 the lidar point cloud for the formation types in Cerrado (Fig. 6.a1-a3). The

485 grasslands observed in the four selected study areas were usually found and  
 486 arranged in small patches among both forests and savannas. Grasslands showed a  
 487 predominantly regular height distribution over the landscape and showed a very  
 488 high density of herbaceous plants per unit area, which makes lidar returns'  
 489 penetration difficult. In savanna formations, UAV-lidar vegetation height  
 490 exceeded 10 m and showed higher structural variability than grasslands (Fig. 6.b1-  
 491 6.c1). The lidar height returns were sparsely and randomly distributed within  
 492 shrubs and isolated trees (Fig. 6.b3). In forests, the lidar height returns were more  
 493 distributed between the lowest and topmost height strata showing two to three  
 494 well-defined canopy strata (Fig. 6.c3).



495  
 496 **Figure 6.** Ground pictures were taken during the field measurements (a-c1). 3-D  
 497 point cloud perspectives for selected sample plots surveyed by UAV-lidar and  
 498 where different biophysical properties were measured (a-c2). Density plots of lidar

499 height returns for the three major formations (a-c3). The letter indicates the  
 500 vegetation formation and is identified as grassland (letters starting with a),  
 501 savanna (letters starting with b), and forest (letter s starting with c).

### 502 3.2. Model performance assessment

503 Table 3 shows five models tested in this study based on the five selected  
 504 lidar metrics (H98TH, COV, H50TH, HKUR, and HSKE). The first model contains  
 505 only the metric H98TH, while for the other models we increased the number of  
 506 variables by adding the remaining lidar metrics, only one per model, based on the  
 507 exhaustive variable selection approach.

508 The best model for estimating AGBt used H98TH and COV only, as they  
 509 were the best predictors among the suite of lidar metrics (Table 3). This model  
 510 produced the lowest AICc and satisfied residual normality and homoscedasticity  
 511 assumptions based on the Shapiro–Wilk ( $W = 0.95$  and  $p\text{-value} = 0.07$ ) and  
 512 Breusch–Pagan ( $BP > 1.47$  and  $p\text{-value} > 0.48$ ) tests.

513

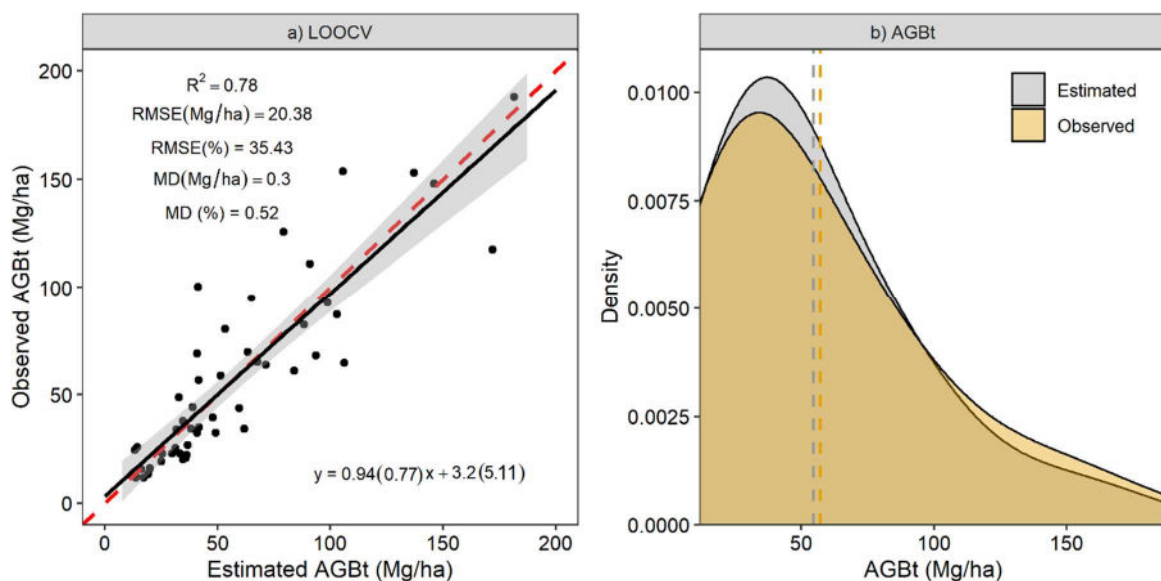
514 **Table 3.** Comparison of calibrated models using UAV-lidar derived metrics for  
 515 estimating total aboveground biomass (AGBt) in Cerrado. The description of the  
 516 UAV-lidar-derived metrics is shown in Table 2.

| Predictors                    | Adj.R <sup>2</sup> | RMSE<br>(Mg/ha) | RMSE<br>(%) | MD<br>(Mg/ha) | MD<br>(%) | AICc  |
|-------------------------------|--------------------|-----------------|-------------|---------------|-----------|-------|
| H98TH                         | 0.74               | 24.30           | 42.46       | -1.79         | -3.12     | 44.11 |
| H98TH, COV                    | 0.79               | 19.11           | 33.40       | -0.26         | -0.46     | 36.49 |
| H98TH, COV, H50TH             | 0.77               | 20.25           | 35.40       | -0.70         | -1.23     | 42.59 |
| H98TH, COV, H50TH, HKUR       | 0.77               | 19.88           | 34.75       | -0.59         | -1.02     | 51.71 |
| H98TH, COV, H50TH, HKUR, HSKE | 0.76               | 20.14           | 35.21       | -0.60         | -1.05     | 63.13 |

517 Note: Adjusted coefficient of determination ( $Adj.R^2$ ), absolute (Mg/ha) and relative  
518 (%) root mean square error (RMSE) and mean differences (MD); Akaike's  
519 information criterion corrected for a small sample size (AICc).

520 Fig. 7a shows the performance of the best model using the H98TH and COV  
521 predictors with the LOOCV procedure. Fig. 7b shows the distribution of the  
522 estimated vs. observed AGBt derived from the LOOCV. Based on the LOOCV  
523 results for the best model (Fig. 7a-b), the model slightly underestimated AGBt over  
524 lower intervals, and slightly overestimated AGBt in higher intervals. Nevertheless,  
525 despite the small differences, the model accuracy as assessed by the LOOCV  
526 procedure showed estimates with a MD less than 1 Mg/ha ( $< 1\%$ ), which reveals  
527 the robustness of the selected model. According to the Wilcoxon rank sum test, the  
528 AGBt estimates derived from LOOCV did not significantly differ from the  
529 observed values (p-value = 0.6918).

530



532

533 **Figure. 7.** (a) Scatterplot of cross-validation predictions versus observations (N=50)  
534 for the natural-logarithm-transformed total aboveground biomass (AGBt) using  
535 the leave-one-out cross-validation (LOOCV). The dashed red line indicates the 1:1  
536 relationship, whereas the black line indicates the best fit. Numbers in parentheses  
are the standard errors for each coefficient. (b) Frequency distribution of both the

537 estimated and the observed distribution of the AGBt. The dashed line indicates the  
 538 mean AGBt for both datasets.

539

540 Table 4 shows AGBt estimation accuracies from both the calibration and  
 541 LOOCV procedures by applying the best model summarized by the Cerrado  
 542 formations. In general, the estimated accuracy of the calibrated model and LOOCV  
 543 showed similar trends, although as expected cross-validation performed slightly  
 544 worse based on relative RMSE and MD. Perhaps due to the sample size (n), the  
 545 grassland model showed the lowest precision (%RMSE) and accuracy (%MD)  
 546 compared to the savanna and forest models. The forest model was most precise  
 547 (lowest %RMSE) while the savanna model was most accurate (lowest %MD).

548

549 **Table 4.** Summary of absolute and relative RMSE for the calibrated model and  
 550 LOOCV AGBt predictions stratified by vegetation formations in Cerrado. n=  
 551 number of observations (field plots) per formation.

| Model                | Formation | RMSE  |       | MD    |       | n  |
|----------------------|-----------|-------|-------|-------|-------|----|
|                      |           | Mg/ha | %     | Mg/ha | %     |    |
| Calibration<br>model | Grassland | 7.16  | 41.63 | 2.52  | 14.65 | 5  |
|                      | Savanna   | 17.24 | 42.69 | -0.17 | -0.43 | 30 |
|                      | Forest    | 24.61 | 23.62 | -1.37 | -1.32 | 15 |
| LOOCV                | Grassland | 7.72  | 44.92 | 2.71  | 15.74 | 5  |
|                      | Savanna   | 17.76 | 43.96 | -0.28 | -0.68 | 30 |
|                      | Forest    | 27.08 | 25.99 | -1.34 | -1.29 | 15 |

552

553

554

555

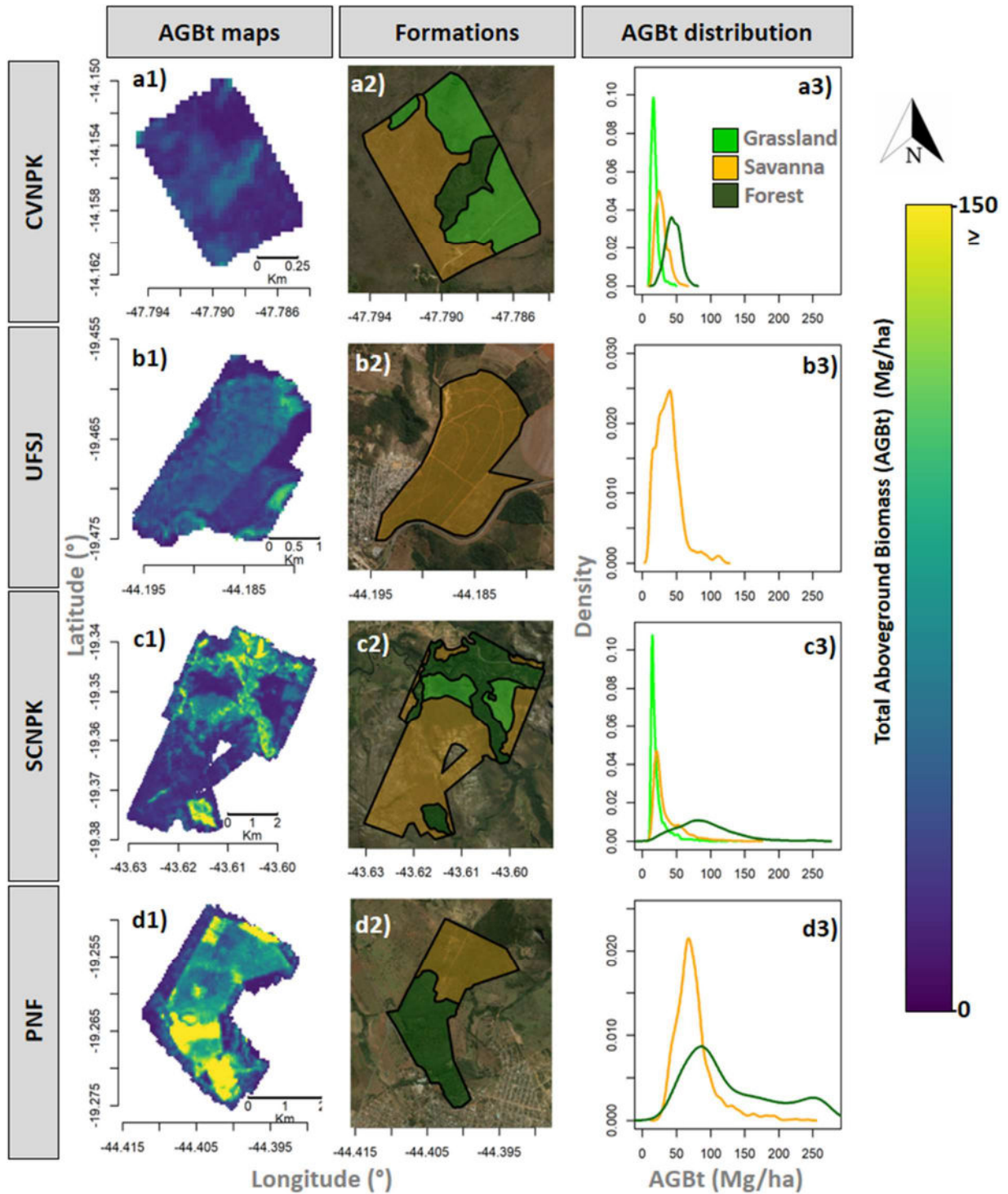
556

### 557 **3.3. Aboveground biomass mapping**

558         The best model was applied across the landscape for mapping AGBt for the  
559 four selected study areas (Fig 8 a1-d1). At the landscape level and according to the  
560 given vegetation formation, the estimated mean and standard error of the AGBt  
561 estimates ranged from 21.28 to 99.35 Mg/ha and 9.03 to 25.39 Mg/ha, respectively  
562 (Table 5). Savanna and forest formations stored 48.09% (19.72 Mg/ha) and 78.58%  
563 (78.07 Mg/ha) more AGBt than grassland within our study sites. The uncertainty  
564 associated with the AGBt estimated mean was higher in the grassland than in  
565 savanna or forest formations (Table 5). In terms of spatial coverage, savanna was  
566 the most predominant contributing vegetation formation in the four study sites,  
567 which encompassed 59.8% of the total area, followed by forests (30.7%) and  
568 grassland (9.5%).

569         The use of high spatial resolution data from both GatorEye UAV-RGB and  
570 PlanetScope imagery allows for the delineation of the spatial distribution of each  
571 Cerrado formation for the four selected study areas (Fig. 8). Two sites showed all  
572 three vegetation formations (Fig 8a2, and c2), whereas one site showed both  
573 savanna and forest formations (Fig. 8d2), and one site only savanna (Fig 8c2). The  
574 resulting histograms show the proportions of AGBt for each study site and  
575 Cerrado formation (Fig 8 a3-d3).

576



577

578 **Figure 8.** UAV-lidar derived maps of total aboveground biomass (AGBt) for the  
 579 study sites a1-d1) with 30 m spatial resolution; Cerrado formation layers a2-d2)  
 580 and distribution of the AGBt per vegetation formation in Cerrado.

581

582 **Table 5.** Summary of the total aboveground biomass (AGBt) and variance  
 583 estimators at the landscape scale within the Cerrado formations. n = number of  
 584 observations (mapped grid cells).

| Formation | $\widehat{E}(\mu)$ | $V[\widehat{E}(\mu)]$ | $\widehat{SE}$ | $\% \widehat{SE}$ | n      |
|-----------|--------------------|-----------------------|----------------|-------------------|--------|
| Grassland | 21.28              | 25.39                 | 5.04           | 23.68             | 1,578  |
| Savanna   | 41.00              | 9.03                  | 3.00           | 7.33              | 10,044 |
| Forest    | 99.35              | 15.64                 | 3.95           | 3.98              | 5,160  |

585

#### 586 4. Discussion

587 Cerrado is the second-largest source of carbon emissions in Brazil ([Metzger](#)  
 588 [et al. 2019](#)), and hence accurate measurements of AGBt are crucial for boosting  
 589 vegetation carbon management, conservation, and restoration initiatives ([Bispo](#)  
 590 [et al., 2020](#)). Our study demonstrates, for the first time, the potential of high-density  
 591 UAV lidar sensors and the resultant 3-D point clouds to accurately capture the  
 592 highly heterogeneous structure of tropical savanna in Brazil, which is  
 593 characterized by the presence of various vegetation formations, including  
 594 grassland, savanna, and forest. Thus, it is possible to model the AGBt, which also  
 595 accounts for the contribution of small trees, shrubs, and surface vegetation to total  
 596 biomass, as opposed to the majority of studies that have focused on only the  
 597 woody AGB of the canopy (e.g., [Bispo et al., 2020](#); [Zimbres et al., 2020](#)).

598

#### 599 4.1 Including non-woody vegetation in lidar estimations of aboveground 600 biomass

601 The lidar-assisted estimation of biomass of non-woody vegetation is  
 602 relatively neglected in the scientific literature, despite its large proportional  
 603 contribution to global carbon flux from biomass burning ([van der Werf et al., 2010](#);  
 604 [Poulter et al., 2014](#); [Pugh et al. 2019](#); [Duvert et al., 2020](#); [Lasslop et al., 2020](#)).  
 605 Although there are numerous studies regarding the use of lidar to estimate and

606 monitor forest structure and AGB in a range of biomes and vegetation types (e.g.  
607 [Clark et al., 2011](#); [Hudak et al. 2012](#); [Andersen et al., 2013](#); [Asner and Mascaro,](#)  
608 [2014](#); [Silva et al., 2017](#)), there is a scarcity of studies that include the full range of  
609 vegetation formations found in the Cerrado biome. Our results are not truly  
610 comparable to model performances obtained by other studies using lidar for  
611 biomass mapping in tropical savanna ecosystems, because those typically targeted  
612 only woody AGB (e.g. [Bispo et al., 2020](#); [Zimbres et al., 2020](#)) as opposed to the  
613 AGBt estimation done in our study. For instance, [Levick et al. \(2019\)](#), using ALS  
614 for assessing habitat structure and woody aboveground carbon (AGC) response to  
615 altered fire regimes in tropical savanna in Australia, were able to calibrate models  
616 and map AGC to the entire experimental site with model performance resulting in  
617 a  $R^2$  of 0.82 and RMSE of 7.35 Mg/ha; the absolute RMSE (Mg/ha) would  
618 approximately double in terms of AGB. [Bispo et al. \(2020\)](#), also using ALS derived  
619 top canopy height and cover metrics for estimating only woody AGB, showed  
620 good model performance with  $R^2$  of 0.93 and RMSE of 6.74 Mg/ha (13.0%).  
621 [Almeida et al. \(2019\)](#) used the same GatorEye UAV-lidar system presented in this  
622 study, but in a tropical forest ecosystem, and were able map AGB across different  
623 forest successional stages with model performance  $R^2$  of 0.80 and RMSE of 24.9  
624 Mg/ha (9.0%), respectively. The fact that the performance of our models was  
625 slightly worse than those presented by these authors can be explained by our  
626 approach to include non-woody vegetation in our estimation of AGBt, not just  
627 AGB stored in trees; although lidar is sensitive to woody canopy structure, its  
628 sensitivity to understory and surface fuel components, particularly the litter layer  
629 at ground level, is diminished, thus contributing to larger estimation errors. For  
630 instance, [Bispo et al. \(2020\)](#) did not include data from grassland formations in their  
631 Cerrado gradient, which is the type of vegetation formation that typically yields  
632 higher errors in studies concurring to our results ([Wang et al. 2017](#); [Marselis et al.,](#)  
633 [2018](#); [Zhang et al. 2018](#); [Madsen et al., 2020](#)). If shrubs and surface vegetation are

634 not included in the sample, the resulting models cannot be extrapolated to map  
635 AGB toward grassland areas, which can be quite a representative proportion of the  
636 land in savanna ecosystems like Cerrado (Fig. 8). In turn, our results demonstrate  
637 that the estimation of AGBt is possible at a level of certainty comparable to  
638 estimating AGB from trees alone, which makes worth the extra effort in the  
639 sampling protocol compared to the gain obtained when including a proportionally  
640 relevant component of total vegetation biomass. Given the high importance of  
641 grassland estimation in savanna biomes (Simon et al., 2009), and their importance  
642 to global carbon balances (van der Werf et al., 2010; Poulter et al., 2014; Pugh et al.  
643 2019; Duvert et al., 2020; Lasslop et al., 2020), it is crucial that further research on  
644 lidar estimations of biomass includes non-woody vegetation formations in both  
645 the sampling and modelling of AGBt.

646

#### 647 **4.2 Convergence on metrics across sensors, platforms, and savanna vegetation** 648 **formations**

649 We were able to identify the best UAV-lidar derived metrics to produce  
650 models that can accurately estimate the distribution of AGBt across the different  
651 vegetation formations, estimate total AGB at plot level, and produce maps at the  
652 landscape level for different regions of the Cerrado. The best model derived by  
653 exhaustive variable selection algorithm uses metrics that represent canopy height  
654 and cover (e.g., H98TH and COV), which concurs with other results for AGB  
655 estimation in tropical ecosystems, including Cerrado (Levick et al. 2019; Bispo et  
656 al., 2020; Zimbres et al., 2020). For instance, Levick et al. 2019 were able to  
657 accurately map woody aboveground carbon (AGC) in tropical savanna in  
658 Australia using only lidar-derived canopy height and cover metrics. Bispo et al.  
659 (2020) used ALS for woody AGB mapping in Cerrado and found that models  
660 calibrated with canopy top height and cover metrics resulted in better  
661 performance. Moreover, lidar-derived top canopy height and cover have been

662 shown to be stable metrics at reduced pulse densities (Hensen et al., 2015; Silva et  
663 al., 2017b), which enables the comparability of different surveys and thus the use  
664 of lidar time series (Bater et al., 2011; Hudak et al. 2012; Cao et al., 2016; Zhao et al.,  
665 2018; Hu et al. 2019). The scientific literature is clearly converging toward the use  
666 of these metrics, and thus they are already considered as standard ecosystem  
667 morphological traits to measure across multiple biomes and data sources  
668 (Valbuena et al., 2020). Our results show that these are also relevant in gradients  
669 including both forests and grassland ecosystems, which has great global  
670 implications (Simon et al., 2009). This convergence is enabling comparative meta-  
671 analyses across different types of 3-D remote sensing methods, to adequately  
672 assess different landscapes consistently (Valbuena et al., 2020). Thus, vegetation  
673 high (Asner and Mascaró, 2014) and cover (Tang et al., 2019) are as relevant to use  
674 for biomass estimation in grassland-dominated biomes as they are in forests.

675

### 676 **4.3 Overcoming challenges in mapping total aboveground tropical savanna** 677 **ecosystems**

678 The complex physiognomy of ecosystems found in areas like Cerrado  
679 creates particular challenges to mapping biomass distributions using remote  
680 sensing. For this reason, there is only limited literature regarding the use of remote  
681 sensing to estimate AGBt, as compared to woody AGB estimation in savannas  
682 (Levick et al. 2019; Bispo et al., 2020; Zimbres et al., 2020). Accurate maps of AGBt  
683 can however help to identify the distributions of the different vegetation  
684 formations across the landscape, and their associated uncertainties. Our study thus  
685 serves as a benchmark for further data collection and could enable large scale  
686 availability of baseline data regarding Cerrado biome biomass stores. The accuracy  
687 of AGBt estimation varied across different vegetation formations, with relatively  
688 greater uncertainty observed in grassland formations. This result may be attributed  
689 to the smaller sample size for grassland and also the limitations of lidar (not just

690 UAV platforms) in capturing the 3-D structure for this formation. The high density  
691 of low-lying vegetation in the grassland, which lowers penetration of lidar pulses,  
692 can negatively impact the ability to differentiate vegetation returns from ground  
693 returns (Hopkinson et al. 2004; Streutker et al. 2006), introducing further errors  
694 and increasing the uncertainty. Such complications likely contribute to the  
695 apparent shortage of literature regarding the study of grassland vegetation with  
696 lidar (Hudak et al. 2016). Further research should focus more on including the  
697 grassland areas with a stratified design (Adnan et al. 2021), since grassland areas  
698 are characterized by low AGBt values that may be undersampled in study designs.  
699

#### 700 **4.4 Wider implications of our findings**

701 The findings of this study, together with further research on this topic, can  
702 assist in the development of more accurate carbon monitoring and integrated fuel  
703 and fire management activities in Cerrado. For example, while developing maps of  
704 broad coverage, UAV-lidar can provide data for calibration and validation of  
705 satellite-based biomass maps, which are increasingly used owing to the  
706 proliferation of open-source platforms. Another critical and real-time application  
707 of UAV-lidar AGB maps are for validating satellite products, such as those from  
708 NASA's GEDI and ICESat-2 (Ice, Cloud, and land Elevation Satellite 2) missions  
709 (Silva et al., 2021). Consequently, UAV-lidar presents a convenient, relatively low-  
710 cost solution to collect data with an extremely high point density, thereby  
711 capturing and describing structural differences in the Cerrado. In tandem, these  
712 allow for the generation of locally highly accurate estimates of total AGB for  
713 specific Cerrado formations. The need for high-resolution assessments to calibrate  
714 and validate satellite-based biomass maps is crucial in the face of the enormous  
715 pressure that local and global changes are exerting on Cerrado. For instance,  
716 employing maps with higher uncertainty in grassland might limit or hinder the  
717 predictive capability of ongoing fire management strategies at Cerrado and

718 warrant urgent attention in terms of their implications for practical applications.  
719 Currently, however, there is no better alternative in terms of speed and cost for  
720 large-scale estimation of AGBt in Cerrado, and so it may be the case that the  
721 greater quantities of UAV-lidar data and coverage compared to field  
722 measurements compensate for a slightly higher uncertainty in the predictions,  
723 especially in grassland formations.

724

#### 725 **4.5 Future directions**

726 It is expensive and challenging to conduct fieldwork in the Brazilian  
727 Cerrado, and existing field datasets still do not entirely represent the extent and  
728 complexity of the biome. This study has demonstrated UAV-lidar can successfully  
729 describe Cerrado vegetation formations over large areas and has the potential to  
730 dramatically increase the size and accuracy of datasets commonly used to classify  
731 (and misclassify) Cerrado vegetation types in large scale satellites-derived AGB  
732 maps. The development of AGB mapping techniques as demonstrated in this  
733 study will have a strong impact on our ability to map and monitor AGB in the  
734 Cerrado biome, particularly with regards to the often-overlooked surface biomass.  
735 Nonetheless, the observed uncertainty in grassland should be investigated in  
736 depth in future studies for improving AGB mapping accuracy, and for achieving  
737 this goal, we recommend testing the possibility of integrating TLS with UAV-lidar,  
738 as well as evaluating the stand-alone accuracy of TLS techniques ([Zimbres et al.](#)  
739 [2020](#)). Moreover, with increased study of and field inventories in grassland  
740 formations, we could expand our data repository and increase surface biomass  
741 estimation accuracies; this will also allow forest managers to determine the  
742 minimum number of field plots required for estimating surface biomass in a  
743 satisfactory manner and help optimize field data collection costs. Future work that  
744 uses the workflows and outputs presented in this study to derive large scale, wall-  
745 to-wall AGBt maps have potential to greatly contribute to improvements in carbon

746 monitoring, and integrated fire and wildfire management. As the accuracy of  
747 remote sensing techniques improves, it may be that this study has provided a  
748 benchmark against which to show improvements in AGBt estimation for  
749 monitoring of carbon and wildfire management.

750

## 751 **5. Conclusion**

752 In this study, the use of UAV-lidar allowed us to accurately derive different  
753 vegetation metrics from 3-D point clouds to model and estimate total aboveground  
754 biomass at the landscape scale across the Cerrado formations at moderate-  
755 resolution. Our methodological approach may be upscaled to larger areas with  
756 success as it covers the main vegetation types of the biome, consisting of a gradient  
757 from grasslands to savannas and forests. Our modeling analysis identified the best  
758 lidar-derived metrics to use to estimate total aboveground biomass, where  
759 dominant vegetation height and canopy cover were the variables that showed the  
760 best model performance. The biomass map and framework presented in this paper  
761 can complement field assessments, and calibrate and validate other methods to  
762 estimate total aboveground biomass based on satellite data, such as GEDI. In this  
763 sense, users may potentially improve the spatial and temporal resolution of  
764 aboveground biomass monitoring in a region, which plays a key role in the global  
765 carbon cycle and where the distribution of total aboveground biomass is still  
766 unquantified. The study findings may support new decision support systems  
767 based on accurate monitoring of aboveground biomass aiming to inform and  
768 improve forest policy responses concerning issues of forest degradation, carbon  
769 emissions, and ecosystem function. Additionally, the outcomes of this research can  
770 support future research to advance understanding of climate-fire interactions and  
771 the mutual feedbacks between changing fire regimes and fuel biomass.

772

773

774

775 **Acknowledgments**

776 This project was supported by the Brazilian National Council for Scientific  
777 and Technological Development (CNPq, grant 442640/2018-8, CNPq/Prevfogo-  
778 Ibama N<sup>o</sup> 33/2018) and NASA's Carbon Monitoring System (CMS, grant 20-  
779 CMS20-0036). D. R.A.A. was supported by the São Paulo Research Foundation  
780 (#2018/21338-3). A.C. was financed in part by MCTIC/CNPq N<sup>o</sup> 28/2018  
781 (#408785/2018-7; #438875/2018-4), CNPq N<sup>o</sup> 09/2018 (#302891/2018-8). This study  
782 was financed in part by the Coordenação de Aperfeiçoamento de Pessoal de Nível  
783 Superior – Brasil (CAPES) – Finance Code 001. M.E.F. is a CNPq Research Fellow  
784 (grant #315699/2020-5). We gratefully acknowledge the following undergraduate  
785 and graduate students involved in the field work campaign: Alberto A. Gontijo e  
786 Silva, Alexandre S. C. Filho, André Felipe C. Lima, Bernardo dos S. de Almeida,  
787 Carlos Magno M. de Oliveira, Gilberto do A. Pacheco; Gustavo R. Lattanzi, Iago  
788 Henrique F. da Silva, Irene M. Barbosa, Ivo S. Moreira, Jacson A. A. Machado,  
789 Jean Victor N. Paiva, Junia S. M. Macedo, Leandra Dietrich, Lídia A. de Aguiar,  
790 Matheus Gunther M. Soares, Nelson Amaral, Nivaldo R. J. Junior, Reginaldo  
791 Arthur G. Marcelino, Thiago Trajano. Moreover, we thank the park managers:  
792 Edward Elias Junior, Celso Lago-Paiva and Leandro Chagas from the Serra do  
793 Cipó National Park, Maria Carolina A. Camargos from the Chapada dos Veadeiros  
794 National Park and Renato Diniz Dumont from the Paraopeba National Forest.  
795 GatorEye data collection and processing by AMAZ and ENB was supported in  
796 part by the McIntire-Stennis program of the USDA, and the School of Forest  
797 Resources and Conservation and the Center for Latin America Studies at UFL.  
798 Finally, we would like to thank the editors and two reviewers for providing  
799 constructive comments to improve the quality of the manuscript.

800

801 **Author Contributions:**

802 M.B.T.C., C.A.S and R.V.L. designed the study. M.B.T.C., C.A.S, R.V.L.,  
803 A.L.S., L.R.G., V.A.C., D.R.A.A., A.H. and C.K. collected and processed the AGBt  
804 field data. E.N.B. and A.M.A.Z. collected and processed the UAV-lidar data. R.V.,  
805 B.L.F., C.S.J., M.E.F., J.L., S.P.C.C., J.S. and A.C., C.H.A., contributed with the  
806 methodological framework, data processing analysis and write up. C.K., A.H.,  
807 L.A., J.J., E.F., C.H.A., and M.E.F. contributed to the interpretation, quality control  
808 and revisions of the manuscript. All authors read and approved the final version  
809 of the manuscript.

## 810 **References**

811 Adnan, S., Maltamo, M., Packalen, P., Mehtätalo, L., Ammataro, N., Valbuena, R.  
812 (2021). Determining maximum entropy in 3D remote sensing height distributions  
813 and using it to improve aboveground biomass modelling via stratification.  
814 (Submitted to Remote Sensing of Environment). Accessed Jan. 02 2021. Retrieved  
815 from <https://dissertationesforestales.fi/pdf/article10467.pdf>

816 Akaike, H. (1979). A Bayesian extension of the minimum AIC procedure of  
817 autoregressive model fitting. *Biometrika*, 66, (2), 237-242.  
818 <https://doi.org/10.1093/biomet/66.2.237>.

819 Almeida, DRA., Broadbent, EN., Zambrano, A. M. A., Wilkinson, BE., Ferreira,  
820 ME., Chazdon, R., Melia, P., Gorgense, EB., Silva, CA., Starkg, SC., Valbuena, R.,  
821 Papa, DA., Brancalion, PHS. (2019). Monitoring the structure of forest restoration  
822 plantations with a drone-lidar system. *International Journal of Applied Earth*  
823 *Observation and Geoinformation*, 79, 192-198. <https://doi.org/10.1016/j.jag.2019.03.014>

824 Almeida, DRA., Almeyda Zambrano, AM., Broadbent, EN., Wendt, AL., Foster, P.,  
825 Wilkinson, B. E., Salk, C., Papa, DA., Stark, SC., Valbuena, R., Gorgens, E. B., Silva,  
826 C. A., Brancalion, PHS., Fagan, M., Meli, P., Chazdon, R. (2020). Detecting  
827 successional changes in tropical forest structure using GatorEye drone-borne lidar.  
828 *Biotropica*, 52 (6), 1156-1168. <https://doi.org/10.1111/btp.12814>

829 Alvarado, ST., Fornazari, T., Cóstola, A., Morellato, LPC., Silva, TSF. (2017).  
830 Drivers of fire occurrence in a mountainous Brazilian cerrado savanna: Tracking  
831 long-term fire regimes using remote sensing. *Ecological Indicators*, 78 (1), 270-281.  
832 <https://doi.org/10.1016/j.ecolind.2017.02.037>

833 Alvares, CA., Stape, JL., Sentelhas, PC., De Moraes Gonçalves, JL., Sparovek, G.  
834 (2013) Köppen's climate classification map for Brazil. *Meteorologische Zeitschrift*, 22  
835 (6), 711-728.

836 Andersen, H., Reutebuch, S. E., Mcgaughey, R. J., Oliveira, MVN., Keller, M.  
837 (2013). Monitoring selective logging in western Amazonia with repeat lidar flights.  
838 *Remote Sensing of Environment*, 151, 157-165. <https://doi.org/10.1016/j.rse.2013.08.049>

839 Anderson, KE., Glenn, NF., Spaete, LP., Shinneman, DJ., Pilliod, DS., Arkle, RS.,  
840 McIlroy, SK., Derryberry, DR. (2018). Estimating vegetation biomass and cover  
841 across large plots in shrub and grass dominated drylands using terrestrial lidar  
842 and machine learning. *Ecological Indicators*, 84, 793-802.  
843 <https://doi.org/10.1016/j.ecolind.2017.09.034>

844 Araújo, FM., Ferreira, LG., Arantes, AE. (2012). Distribution patterns of burned  
845 areas in the Brazilian Biomes: An analysis based on satellite data for the 2002-2010  
846 period. *Remote Sensing*, 4 (7), 1929-1946. <https://doi.org/10.3390/rs4071929>

847 Asner, GP., Mascaro, J. (2014). Mapping tropical forest carbon: Calibrating plot  
848 estimates to a simple LiDAR metric. *Remote Sensing of Environment*, 140, 614-624.  
849 <https://doi.org/10.1016/j.rse.2013.09.023>

850 Balduino, APDC., Souza, ALD., Meira Neto, JAA., Silva, AFD., Silva Júnior, MCD.  
851 (2005). Phytosociological composition and floristic comparison of cerrado of  
852 Paraopeba flora-MG. *Revista Árvore*, 29 (1), 25-34. [https://doi.org/10.1590/S0100-](https://doi.org/10.1590/S0100-67622005000100004)  
853 [67622005000100004](https://doi.org/10.1590/S0100-67622005000100004)

854 Bater, CW.; Wulder, MA.; Coops, NC.; Nelson, RF.; Hilker, T.; Naesset, E. (2011).  
855 Stability of sample-based scanning-lidar-derived vegetation metrics for forest  
856 monitoring. *IEEE Transactions on Geoscience and Remote Sensing*, 49 (6), 2385-2392.  
857 <https://doi.org/10.1109/TGRS.2010.2099232>

858 Benites, VM., Caiafa AN., Mendonça, ES., Schaefer CEGR., Ker, JC. (2003). Solos e  
859 vegetação nos Complexos Rupestres de Altitude da Mantiqueira e do Espinhaço.  
860 *Floresta e Ambiente*, 10 (1), 76-85.

861 Bispo, PC., Rodríguez-Veiga, P., Zimbres, B., Do Couto De Miranda, S., Cezare,  
862 CHG., Fleming, S., Badalchhino, F., Louis, V., Rains, D., Garcia, M., Espirito Santo,  
863 MFDB., Roitman, I., Pacheco-Pascagaza, AM., Gou, Y., Roberts, J. Barret, K.,  
864 Ferreira, LG., Shimbo, JZ., Alencar, A., Bustamanete, M., Woodhouse, LH., Sano,  
865 EE., Ometto, JP., Tansey, K., Balzter, H. (2020). Woody aboveground biomass

866 mapping of the brazilian savanna with a multi-sensor and machine learning  
867 approach. *Remote Sensing*, 12 (17), 2685. <https://doi.org/10.3390/rs12172685>

868 Bonanomi, J., Tortato, F. R., Raphael de Souza, R. G., Penha, J. M., Bueno, A. S.,  
869 Peres, C. A. (2019). Protecting forests at the expense of native grasslands: Land-use  
870 policy encourages open-habitat loss in the Brazilian cerrado biome. *Perspectives in  
871 ecology and conservation*, 17(1), 26-31. <https://doi.org/10.1016/j.pecon.2018.12.002>

872 Breusch, TS., Pagan, ARA. (1979). Simple Test for Heteroscedasticity and Random  
873 Coefficient Variation. *Econometrica: Journal of the Econometric Society*, 47 (1), 1287-  
874 1294. <https://doi.org/10.2307/1911963>

875 Broadbent, EN., Zambrano, AMA., Omans, G., Adler, A., Alonso, P., Naylor, D.,  
876 Chenevert, G., Murtha, T., Vogel, J., Almeida, DRA., Dalla Corte, AP., Silva, CA.,  
877 Prata, GA., Merrick, T., D'Oliveira, MVN., Detto, M., Ferreira, MP., Wilkinson, BE.,  
878 Ferreira, ME., Muller-Landau, HC. (2020). In prep. The GatorEye Unmanned  
879 Flying Laboratory: sensor fusion for 4D ecological analysis through custom  
880 hardware and algorithm integration, accessed Set. 10 2020. Retrieved from  
881 <http://www.gatoreye.org>

882 Cao, L., Coops, NC., Innes, JL., Sheppard, SR., Fu, L., Ruan, H., She, G. (2016)  
883 Estimation of forest biomass dynamics in subtropical forests using multi-temporal  
884 airborne LiDAR data. *Remote Sensing of Environment*, 178 (1), 158–171.  
885 <https://doi.org/10.1016/j.rse.2016.03.012>

886 Chave, J., Réjou-Méchain, M., Búrquez, A., Chidumayo, E., Colgan MS., Delitti,  
887 WBC., Duque, A., Eid, T., Fearnside, PM., Goodman, RC., Henry, M., Martínez-  
888 Yrizar, A., Mugasha, WA., Muller-Landau, HC., Mencuccini, M., Nelson, BW.,  
889 Ngomanda, A., Nogueira, EM., Ortiz-Malavassi, E., Pélissier, R., Ploton, P., Ryan,  
890 CM., Saldarriaga, J. G., Vieilledent, G. (2014). Improved allometric models to  
891 estimate the aboveground biomass of tropical trees. *Global Change Biology*, 20 (10),  
892 3177–3190. <https://doi.org/10.1111/gcb.12629>

893 Clark, ML., Roberts, DA., Ewel, JJ., Clark, DB. (2011). Remote Sensing of  
894 Environment Estimation of tropical rain forest aboveground biomass with small-  
895 footprint lidar and hyperspectral sensors. *Remote Sensing of Environment*, 115  
896 (11), 2931–2942. <https://doi.org/10.1016/j.rse.2010.08.029>

897 Dalla Corte, AP., Souza, D. V., Rex, FE., Sanquetta, CR., Mohan, M., Silva, CA.,  
898 Zambrano, AMA, Prata, G., Almeida, DRA., Trautenmuller, JW., Klauberg, C.,  
899 Mpraes, A., Sanquetta, MN., Wilkinson, B., Broadbent, EN. (2020). Forest inventory  
900 with high-density UAV-Lidar: Machine learning approaches for predicting

901 individual tree attributes. *Computers and Electronics in Agriculture*, 179 (1), 105815.  
902 <https://doi.org/10.1016/j.compag.2020.105815>

903 Dass, P., Houlton, BZ., Wang, Y., Warlind, D. (2018). Grasslands may be more  
904 reliable carbon sinks than forests in California. *Environmental Research Letters*, 13  
905 (7), 074027. <https://doi.org/10.1088/1748-9326/aacb39>

906 Drake, JB., Dubayah, RO., Clark, DB., Knox, RG., Blair, JB., Hofton, MA., Prince, S.  
907 (2002). Estimation of tropical forest structural characteristics using large-footprint  
908 coping. *Remote Sensing of Environment*, 79 (2-3), 305-319.  
909 [https://doi.org/10.1016/S0034-4257\(01\)00281-4](https://doi.org/10.1016/S0034-4257(01)00281-4)

910 Dubayah, R., Blair, JB., Goetz, S., Fatoyinbo, L., Hansen, M., Healey, S., Hofton, M.,  
911 Hurtt, G., Kellner, J., Luthcke, S., Armston, J., Tang, H., Duncanson, L., Hancock,  
912 S., Jantz, P., Marselis, S., Patterson, PL., Wenlu, Q., Silva, C. (2020). The Global  
913 Ecosystem Dynamics Investigation: High-resolution laser ranging of the Earth's  
914 forests and topography. *Science of Remote Sensing*, 1, 100002.  
915 <https://doi.org/10.1016/j.srs.2020.100002>

916 Durigan, G., Pilon, NAL., Abreu, RCR., Hoffmann, WA., Martins, M., Fiorillo, BF.,  
917 Antunes, AZ., Carmignotto, AP., Maravalhas, JB., Vieira, J., Vasconcelos, HL.  
918 (2020). No Net Loss of Species Diversity After Prescribed Fires in the Brazilian  
919 Savanna. *Frontiers in Forests and Global Change*, 3 (13), 1-15.  
920 <https://doi.org/10.3389/ffgc.2020.00013>

921 Durigan, G., Ratter, JA. (2016). The need for a consistent fire policy for Cerrado  
922 conservation. *Journal of Applied Ecology*, 53 (1), 11-15. <https://doi.org/10.1111/1365-2664.12559>

924 Duvert, C., Hutley, LB, Beringer, J., Bird, MI, Birkel, C., Maher, DT, Northwood,  
925 M., Rudge, M., Setterfield, SA., Wynn, JG (2020). Balanço líquido de carbono da  
926 paisagem de uma savana tropical: importância relativa do fogo e da exportação  
927 aquática na compensação da produção terrestre. *Global Change Biology*, 26 (10),  
928 5899-5913. <https://doi.org/10.1111/gcb.15287>

929 D'Oliveira, MVN., Broadbent, EN., Oliveira, LC., Almeida, DRA., Papa, DA.,  
930 Ferreira, ME., Zambrano, AMA., Silva, CA., Avino, FS., Prata, GA., Mello, RA.,  
931 Figueiredo, EO., Jorge, LAC., Junior, L., Albuquerque, RW., Brancalion, PHS.,  
932 Wilkinson, B., Oliveira-da-Costa, M. (2020). Aboveground Biomass Estimation in  
933 Amazonian Tropical Forests: a Comparison of Aircraft- and GatorEye UAV-borne  
934 LiDAR Data in the Chico Mendes Extractive Reserve in Acre, Brazil. *Remote  
935 Sensing*, 12 (11), 1754. <https://doi.org/10.3390/rs12111754>

- 936 Felfili, J. M. (2007). Biogeografia do Bioma Cerrado: vegetação e solos da Chapada  
937 dos Veadeiros. (1<sup>a</sup> ed.). UnB: Finatec.
- 938 Ferreira, V., Mateus, L., Aguiar, J. (2012) Site recording using automatic image  
939 based three dimensional reconstruction techniques. *Proceedings of the International*  
940 *Conference on Computer Applications & Quantitative Methods in Archaeology, CAA,*  
941 26–30.
- 942 Flores, BM., de Sá Dechoum, M., Schmidt, IB., Hirota, M., Abrahão, A., Verona, L.,  
943 ... & Pamplona, MB. (2020). Tropical riparian forests in danger from large savanna  
944 wildfires. *Journal of Applied Ecology*, 1 (1). <https://doi.org/10.1111/1365-2664.13794>
- 945 Franke, J., Barradas, ACS., Borges, MA., Menezes Costa, M., Dias, PA., Hoffmann,  
946 AA., Orozco Filho, JC., Melchiori, AE., Siegert, F. (2018). Fuel load mapping in the  
947 Brazilian Cerrado in support of integrated fire management. *Remote Sensing of*  
948 *Environment*, 217 (1), 221–232. <https://doi.org/10.1016/j.rse.2018.08.018>
- 949 García, M., Riaño, D., Chuvieco, E., Danson, FM. (2010). Estimating biomass  
950 carbon stocks for a Mediterranean forest in central Spain using LiDAR height and  
951 intensity data. *Remote Sensing of Environment*, 114 (4), 816-830.  
952 <https://doi.org/10.1016/j.rse.2009.11.021>
- 953 Goldbergs, G., Levick, SR., Lawes, M., Edwards, A. (2018). Hierarchical integration  
954 of individual tree and area-based approaches for savanna biomass uncertainty  
955 estimation from airborne LiDAR. *Remote sensing of environment*, 205 (1), 141-150.  
956 <https://doi.org/10.1016/j.rse.2017.11.010>
- 957 Guimarães, JRC., Rios, PR. (2010). Martensite start temperature and the austenite  
958 grain-size. *Journal of materials science*, 45 (4), 1074-1077.  
959 <https://doi.org/10.1007/s10853-009-4044-0>
- 960 Gwenzi, D., Lefsky, MA. (2016). Spatial modeling of Lidar-derived woody biomass  
961 estimates collected along transects in a heterogeneous savanna landscape. *IEEE*  
962 *Journal of Selected Topics in Applied Earth Observations and Remote Sensing*, 10 (1), 372-  
963 384. <https://doi.org/10.1109/JSTARS.2016.2582148>
- 964 Harkel, JT., Bartholomeus, H., Kooistra, L. (2020). Biomass and crop height  
965 estimation of different crops using UAV-based LiDAR. *Remote Sensing*, 12 (1), 17.  
966 <https://doi.org/10.3390/rs12010017>
- 967 Hansen, E.H.; Gobakken, T.; Næsset, E. Effects of Pulse Density on Digital Terrain  
968 Models and Canopy Metrics Using Airborne Laser Scanning in a Tropical  
969 Rainforest. *Remote Sens.* 2015, 7, 8453-8468.

970 Hernando, A., Velázquez, J., Valbuena, R., Legrand, M., García-Abril, A. (2017).  
971 Influence of the resolution of forest cover maps in evaluating fragmentation and  
972 connectivity to assess habitat conservation status. *Ecological Indicators*, 79, 295-302.  
973 <https://doi.org/10.1016/j.ecolind.2017.04.031>

974 Hirota, M., Holmgren, M., Van Nes, EH., Scheffer, M. (2011). Global resilience of  
975 tropical forest and savanna to critical transitions. *Science*, 334 (6053), 232-235.  
976 <https://doi.org/10.1126 / science.1210657>

977 Hu, T., Ma, Q., Su, Y., Battles, JJ., Collins, BM., Stephens, SL., Kelly, M., Guo, Q.  
978 (2019). A simple and integrated approach for fire severity assessment using bi-  
979 temporal airborne LiDAR data. *International Journal of Applied Earth Observation and*  
980 *Geoinformation*, 78, 25-38. <https://doi.org/10.1016/j.jag.2019.01.007>

981 Hudak, AT., Crookston, NL., Evans, JS., Falkowski, MJ., Smith, AM., Gessler, PE.,  
982 Morgan, P. (2006). Regression modeling and mapping of coniferous forest basal  
983 area and tree density from discrete-return lidar and multispectral satellite data.  
984 *Canadian Journal of Remote Sensing*, 32 (2), 126-138. <https://doi.org/10.5589/m06-007>

985 Hudak, AT., Strand, EK., Vierling, LA., Byrne, JC., Eitel, JUH., Martinuzzi, S.,  
986 Falkowski, MJ. (2012). Quantifying aboveground forest carbon pools and fluxes  
987 from repeat LiDAR surveys. *Remote Sensing of Environment*, 123 (1), 25–40.  
988 <https://doi.org/10.1016/j.rse.2012.02.023>

989 Hudak, AT., Dickinson, MB., Bright, BC., Kremens, RL., Loudermilk, EL., O'Brien,  
990 JJ., Ottmar, RD. (2016) Measurements relating fire radiative energy density and  
991 surface fuel consumption—RxCADRE 2011 and 2012. *International Journal of*  
992 *Wildland Fire*, 25 (1), 25-37. <https://doi.org/10.1071/WF14159>.

993 Hudak, AT., Fekety, PA., Kane, VR., Kennedy, RE., Filippelli, SK., Falkowski, MJ.,  
994 Tinkham, WT., Smith, AMS., Crookston, NL., Domke, GM. (2020). A carbon  
995 monitoring system for mapping regional, annual aboveground biomass across the  
996 northwestern USA. *Environmental Research Letters*, 15 (9), 095003.  
997 <https://doi.org/10.1088/1748-9326/ab93f9>.

998 Hopkinson, C., Chasmer, LE., Zsigovics, G., Creed, IF., Sitar, M., Treitz, P., Maher,  
999 RV. (2004). Errors in LiDAR ground elevation and wetland vegetation height  
1000 estimates. *International Archives of Photogrammetry, Remote Sensing, and Spatial*  
1001 *Information Sciences*, 36 (8), 108-113.

- 1002 Ibama. (1998). Parque Nacional da Chapada dos Veadeiros: Plano de manejo – Fase  
1003 3 (versão preliminar). (1ª ed.). Ibama.
- 1004 Isenburg, M. (2020). LAStools—Efficient Tools for Lidar Processing. Accessed Dez.  
1005 16 2020. Retrieved from <http://www.cs.unc.edu/~isenburg/lastools/>
- 1006 Lasslop, G., Hantson, S., Harrison, SP., Bachelet, D., Burton, C., Forkel, M., Forrest,  
1007 M., Li, F., Melton, JR., Yue, C., Archibald, S., Scheiter, S., Arneth, A., Hickler, T.,  
1008 Sitch, S. (2020). Global ecosystems and fire: Multi-model assessment of fire-  
1009 induced tree-cover and carbon storage reduction. *Global Change Biology*, 26, 5027-  
1010 5041.
- 1011 Levick, SR., Shendryk, Y., Setterfield, S., Rossiter-Rachor, N. (2018). Evaluation of  
1012 satellite remote sensing pathways for mapping and monitoring of gamba grass for  
1013 the Savanna Fire Management Methodology. (1ºEds.), *Northern Australia*  
1014 *Environmental Research Portal* (pp. 27) CSIRO and Charles Darwin University.
- 1015 Levick, SR., Richards, AE., Cook, GD., Schatz, J., Guderle, M., Williams, RJ.,  
1016 Subedi, P., Trumbore, SE., Andersen, AN. (2019). Rapid response of habitat  
1017 structure and above-ground carbon storage to altered fire regimes in tropical  
1018 savanna. *Biogeosciences*, 16 (7), 1493–1503. <https://doi.org/10.5194/bg-16-1493-2019>
- 1019 Lindenmayer, DB., Wood, JT., Cunningham, RB., MacGregor, C., Crane, M.,  
1020 Michael, D., Montague-Drake, R., Brown, D., Muntz, R. Gill, AM. (2008). Testing  
1021 hypotheses associated with bird responses to wildfire. *Ecological Applications*, 18  
1022 (8), 1967-1983. <https://doi.org/10.1890/07-1943.1>
- 1023 Luck, L., Hutley, LB., Calders, K., Levick, SR. (2020). Exploring the Variability of  
1024 Tropical Savanna Tree Structural Allometry with Terrestrial Laser Scanning.  
1025 *Remote Sensing*, 12 (23), 3893. <https://doi.org/10.3390/rs12233893>
- 1026 Lumley, T. (2020). Leaps: Regression Subset Selection. Thomas Lumley based on  
1027 Fortran code by Alan Miller. R package version 3.1, accessed Dez. 16 2020.  
1028 Retrieved from <https://CRAN.R-project.org/package=leaps>
- 1029 Madsen, B., Treier, UA., Zlinszky, A, Lucieer, A., Normand, S. (2020). Detecting  
1030 shrub encroachment in seminatural grasslands using UAS LiDAR. *Ecology and*  
1031 *Evolution*, 10 (11), 4876-4902. <https://doi.org/10.1002/ece3.6240>
- 1032 Marselis, SM., Tang, H., Armston, JD., Calders, K., Labrière, N., Dubayah, R.  
1033 (2018). Distinguishing vegetation types with airborne waveform lidar data in a

- 1034 tropical forest-savanna mosaic: A case study in Lopé National Park, Gabon. *Remote*  
1035 *sensing of environment*, 216, 626-634. <https://doi.org/10.1016/j.rse.2018.07.023>
- 1036 Marselis, SM., Tang, H., Armston, J., Abernethy, K., Alonso, A., Barbier, N.,  
1037 Bissiengou, P., Jeffery, K., Kenfack, D., Labrière, N. (2019). Exploring the relation  
1038 between remotely sensed vertical canopy structure and tree species diversity in  
1039 Gabon. *Environmental Research Letters*, 14 (9), 094013. [https://doi.org/10.1088/1748-](https://doi.org/10.1088/1748-9326/ab2dcd)  
1040 9326/ab2dcd
- 1041 Marselis, SM., Abernethy, K., Alonso, A., Armston, J., Baker, TR., Bastin, JF.,  
1042 Bogaert, J., Boyd, DS., Boeckx, P., Burslem, DFRP., Chazdon, R., Clark, DB.,  
1043 Coomes, D., Duncanson, L., Hancock, S., Hill, R., Hopkinson, C., Kearsley, E.,  
1044 Kellner, JR., Kenfack, D., Labrière, N., Lewis, SL., Minor, D., Memiaghe, H.,  
1045 Monteagudo, A., Nilus, R., O'Brien, M., Phillips, OL., Poulsen, J., Tang, H.,  
1046 Verbeeck, H., Dubayah, R. (2020). Evaluating the potential of full-waveform lidar  
1047 for mapping pan-tropical tree species richness. *Global Ecology and Biogeography*, 29  
1048 (10), 1799-1816. <https://doi.org/10.1111/geb.13158>
- 1049 Mohan, M., Silva CA., Klauberg, C., Jat, P., Catts, G., Cardil A., Hudak A., Dia, M.  
1050 (2017). Individual Tree Detection from Unmanned Aerial Vehicle (UAV) Derived  
1051 Canopy Height Model in an Open Canopy Mixed Conifer Forest. *Forests*, 8 (9), 340.  
1052 <https://doi.org/10.3390/rs11101161>
- 1053 Metzger, JP., Bustamante, MM.; Ferreira, J., Fernandes, GW., Librán-Embid, F.,  
1054 Pillar, VD., Prist, PR., Rodrigues, RR.; Vieira, ICG., Overbeck, GE. (2019). Why  
1055 Brazil needs its Legal Reserves. *Perspectives in Ecology and Conservation*, 17 (3), 91-  
1056 103. <https://doi.org/10.1016/j.pecon.2019.07.002>
- 1057 Naasset, E., Gobakken, T. (2008). Estimation of above-and below-ground biomass  
1058 across regions of the boreal forest zone using airborne laser. *Remote Sensing of*  
1059 *Environment*, 112 (6), 3079-3090. <https://doi.org/10.1016/j.rse.2008.03.004>
- 1060 Neri, AV., Schaefer, Ceg. R., Souza, AL., Ferreira-Junior, WG., Meira-Neto, JAA.  
1061 (2013). Pedology and plant physiognomies in the cerrado, Brazil. *Anais da Academia*  
1062 *Brasileira de Ciências*, 85 (1), 87-102. [https://doi.org/10.1590/S0001-](https://doi.org/10.1590/S0001-37652013000100007)  
1063 37652013000100007.
- 1064 Oliveira-Filho, A. T., Ratter, J. (2002). Vegetation physiognomies and woody flora  
1065 of the Cerrado biome. In Oliveira, PS., Marquis, TJ. (Eds.), *The Cerrados of Brazil:*  
1066 *Ecology and natural history of a neotropical savanna* (pp. 91–120). Columbia University  
1067 Press.

1068 Ottmar, RD., Vihnanek, RE., Miranda, HS., Sata, MN., Andrade, SM. (2001). Stereo  
1069 photo series for quantifying cerrado fuels in central Brazil. In: Volume I. (Eds.),  
1070 *United States Department of Agriculture*, (pp. 1-87). Forest Service.

1071 Prata, GA., Broadbent, E.N., de Almeida, DRA., St. Peter, J., Drake, J., Medley, P.,  
1072 Corte, APD., Vogel, J., Sharma, A., Silva, CA., Zambrano, AMA., Valbuena, R.,  
1073 Wilkinson, B. (2020). Single-Pass UAV-Borne GatorEye LiDAR Sampling as a  
1074 Rapid Assessment Method for Surveying Forest Structure. *Remote Sensing*, 12 (24),  
1075 4111. <https://doi.org/10.3390/rs12244111>

1076 Persson, HJ., Ståhl, G. (2020). Characterizing Uncertainty in Forest Remote Sensing  
1077 Studies. *Remote Sensing*, 12 (3), 505. <https://doi.org/10.3390/rs12030505>

1078 Pivello, VR. (2011). The use of fire in the cerrado and Amazonian rainforests of  
1079 Brazil: Past and present. *Fire Ecology*, 7 (1), 24-39.  
1080 <https://doi.org/10.4996/fireecology.0701024>

1081 Planet Team. (2017). Planet Application Program Interface: In Space for Life on  
1082 Earth. San Francisco. Accessed Dez. 8 2020. Retrieved from <https://api.planet.com>

1083 Porto, AC., Linares, JAH., Neto, GBS. (2011). Análise da estrutura e dinâmica da  
1084 paisagem do Parque Nacional da Chapada dos Veadeiros. *Anais do Simpósio*  
1085 *Brasileiro de Sensoriamento Remoto-SBSR*. INPE, 3057.

1086 Poulter, B., Frank, D., Ciais, P., Myneni, RB., Andela, N., Bi, J., Broquet, G.,  
1087 Canadell, JG., Chevallier, F., Liu, YY., Running, S., Stich, S., Van der Wef, GR.  
1088 (2014). Contribution of semi-arid ecosystems to interannual variability of the  
1089 global carbon cycle. *Nature*, 509 (7502), 600-603. <https://doi.org/10.1038/nature13376>

1090 Pugh, TA., Lindeskog, M., Smith, B., Poulter, B., Arneth, A., Haverd, V., Calle, L.  
1091 (2019). Role of forest regrowth in global carbon sink dynamics. *Proceedings of the*  
1092 *National Academy of Sciences*, 116 (10), 4382-4387.  
1093 <https://doi.org/10.1073/pnas.1810512116>

1094 Puliti, S., Saarela, S., Gobakken, T., Stahl, G., Næsset, E. (2018). Combining UAV  
1095 and Sentinel-2 auxiliary data for forest growing stock volume estimation through  
1096 hierarchical model-based inference. *Remote Sensing of Environment*, 204, 485-497.  
1097 <https://doi.org/10.1016/j.rse.2017.10.007>

1098 Qureshi, A., Badola, R., Hussain, SA. (2012). A review of protocols used for  
1099 assessment of carbon stock in forested landscapes. *Environmental Science and Policy*,  
1100 16 (1), 81-89, 2012. <https://doi.org/10.1016/j.envsci.2011.11.001>

- 1101 Reichstein, M., Bahn, M., Ciais, P., Frank, D., Mahecha, MD, Seneviratne, SI,  
1102 Zscheisler, J., Cristã, C., Buchmann, N., Frank, DC., Papale, D., Ramming, A.,  
1103 Smith, P., Thonicke, K., Van Der Velde, M., Vicca, S., Walz, A., Wattenbach, M.  
1104 (2013). Climate extremes and the carbon cycle. *Nature*, 500 (7462), 287-295.  
1105 <https://doi.org/10.1038/nature12350>
- 1106 Ribeiro, JF., Walter, BMT (2008). As principais fitofisionomias do bioma Cerrado.  
1107 In: Sano, SM., Almeida, SP., Ribeiro, JF. (Eds.), *Cerrado: Ecologia e flora* (pp. 151-212).  
1108 Embrapa Informação TeCCológica.
- 1109 Ribeiro, MC., Figueira, JEC. (2017). Uma abordagem histórica do fogo no Parque  
1110 Nacional da Serra do Cipó, Minas Gerais–Brasil. *Biodiversidade Brasileira-BioBrasil*, 1  
1111 (2), 212-227. <https://doi.org/10.37002/biobrasil.v%25vi%25i.96>
- 1112 Ribeiro, SC., Fehrmann, L., Soares, CPB., Jacovine, LAG., Kleinn, C., Gaspar, RO.  
1113 (2011). Above-and belowground biomass in a Brazilian Cerrado. *Forest Ecology and*  
1114 *Management*, 262 (3), 491–499. <https://doi.org/10.1016/j.foreco.2011.04.017>
- 1115 Ribeiro, SC., Jacovine, LAG., Torres, CMME., Souza, AL. (2017) Influence of  
1116 interspecific variation on tree carbon stock of a Brazilian Cerrado. *Revista Árvore*,  
1117 41 (5), 1–11. <https://doi.org/10.1590/1806-90882017000500006>
- 1118 Roitman, I., Bustamante, M. M., Haidar, R. F., Shimbo, J. Z., Abdala, G. C., Eiten,  
1119 G., Lindoso, G. S. (2018). Optimizing biomass estimates of savanna woodland at  
1120 different spatial scales in the Brazilian Cerrado: Re-evaluating allometric equations  
1121 and environmental influences. *PloS one*, 13 (8), 1-21.  
1122 <https://doi.org/10.1371/journal.pone.0196742>
- 1123 Saarela, S., Holm, S., Grafström, A., Schnell, S., NaesseT, E., Gregoire, TG., Nelson,  
1124 RF., Stahl, G. (2016). Hierarchical utilizing three sources of information. *Annals of*  
1125 *Forest Science*, 73 (4), 895–910. <https://doi.org/10.1007/s13595-016-0590-1>
- 1126 Scaranello, MAS., Keller, M., Longo, M., Santos, MN., Leitold, V., Morton, DC.,  
1127 Pinagé, ER., Espírito-Santo, FDB. (2019). Estimation of coarse dead wood stocks in  
1128 intact and degraded forests in the Brazilian Amazon using airborne lidar.  
1129 *Biogeosciences*, 16 (17), 3457-3474. <https://doi.org/10.5194/bg-16-3457-2019>.
- 1130 Schaefer, CE., Cândido, HG., Corrêa, GR., Nunes, JA., Arruda, DM. (2016). Soils  
1131 associated with rupestrian grasslands. In: Fernandes, G.W. (Ed.), *Ecology and*  
1132 *Conservation of Mountaintop Grasslands in Brazil*. Springer, Switzerland, pp. 55–  
1133 69. <http://dx.doi.org/10.1007/978-3-319-29808-53>.
- 1134 Shapiro, SS.; Wilk, MB. (1965). An Analysis of Variance Test for Normality  
1135 (Complete Samples). *Biometrika*, 52 (3,4), 591. <https://doi.org/10.2307/2333709>

- 1136 Shendryk, Y., Sofonia, J., Garrard, R., Rist, Y., Skocaj, D., Thorburn, P. (2020). Fine-  
1137 scale prediction of biomass and leaf nitrogen content in sugarcane using UAV  
1138 LiDAR and multispectral imaging. *International Journal of Applied Earth Observation  
1139 and Geoinformation*, 92, (1), 102177. <https://doi.org/10.1016/j.jag.2020.102177>
- 1140 Silva, JMC., Bates, J. M. (2002). Biogeographic patterns and conservation in the  
1141 South American Cerrado: a tropical savanna hotspot: the Cerrado, which includes  
1142 both forest and savanna habitats, is the second largest South American biome, and  
1143 among the most threatened on the continent. *BioScience*, 52 (3), 225-234.  
1144 [https://doi.org/10.1641/0006-3568\(2002\)052\[0225:BPACIT\]2.0.CO;2](https://doi.org/10.1641/0006-3568(2002)052[0225:BPACIT]2.0.CO;2)
- 1145 Silva, SR., Silva, AP., Munhoz, CB., Silva Jr, M. C., Medeiros, MB. (2001). Guia de  
1146 plantas do Cerrado utilizadas na Chapada dos Veadeiros. (1ª ed.). WWF–Brasil.
- 1147 Silva, CA., Klauberg, C., Carvalho, SPC. E, Hudak, AT., Rodriguez, LCE. (2014).  
1148 Mapping aboveground carbon stocks using LiDAR data in Eucalyptus spp.  
1149 plantations in the state of Sao Paulo, Brazil. *Scientia Forestalis*, 42 (104), 591–604.
- 1150 Silva, CA., Klauberg, C.; Hudak, AT., Vierling, L.A., Jaafar, WSWM., Mohan, M.,  
1151 Garcia, M., Ferraz, A., Cardil, A., Saatchi, S. (2017a). Predicting Stem Total and  
1152 Assortment Volumes in an Industrial *Pinus taeda* L. Forest Plantation Using  
1153 Airborne Laser Scanning Data and Random Forest. *Forests*, 8 (7), 254.  
1154 <https://doi.org/10.3390/f8070254>
- 1155 Silva, C.A.; Hudak, A.T.; Vierling, L.A.; Klauberg, C.; Garcia, M.; Ferraz, A.; Keller,  
1156 M.; Eitel, J.; Saatchi, S (2017b). Impacts of Airborne Lidar Pulse Density on  
1157 Estimating Biomass Stocks and Changes in a Selectively Logged Tropical Forest.  
1158 *Remote Sens*, 9, 1068.
- 1159 Silva, CA., Saatchi, S., Garcia, M., Labriere, N., Klauberg, C., Ferraz, A., Meyer, V.,  
1160 Jeffery, KJ., Abernethy, K., White, L., Zhao, K., Lewis, SL., Hudak, AT. (2018).  
1161 Comparison of small- and large-footprint lidar characterization of tropical forest  
1162 aboveground structure and biomass: A case study from Central Gabon. *IEEE  
1163 Journal of Selected Topics in Applied Earth Observations and Remote Sensing*, 11 (10),  
1164 3512-3526. <https://doi.org/10.1109/JSTARS.2018.2816962>
- 1165 Silva, CA., Duncanson, L., Hancock, S., Neuenschwander, A., Thomas, N., Hofton,  
1166 M., Fatoyinbo, L., Simard, M., Marshak, CZ., Armston, J., Lutchke, S., Dubayah, R.  
1167 (2021) Fusing simulated GEDI, ICESat-2 and NISAR data for regional  
1168 aboveground biomass mapping. *Remote Sensing of Environment*, 253, 112234.  
1169 <https://doi.org/10.1016/j.rse.2020.112234>

1170 Silva, VS., Silva, CA., Mohan, M., Cardil, A., Rex, FE., Loureiro, GH., Almeida,  
1171 DRA., Broadbent, EN., Gorgens, EB., Dalla Corte, AP., Silva, EA., Valbuena, R.,  
1172 Klauberg, C. (2020). Combined Impact of Sample Size and Modeling Approaches  
1173 for Predicting Stem Volume in Eucalyptus spp. Forest Plantations Using Field and  
1174 LiDAR Data. *Remote Sensing*, 12 (9), 1438.

1175 Simon, MF., Grether, R., de Queiroz, LP., Skema, C., Pennington, RT., Hughes, CE.  
1176 (2009). Recent assembly of the Cerrado, a neotropical plant diversity hotspot, by in  
1177 situ evolution of adaptations to fire. *Proceedings of the National Academy of Sciences*,  
1178 106(48), 20359-20364. <https://doi.org/10.1073/pnas.0903410106>

1179 Singh, RK., Kumar, P., Mukherjee, S., Suman, S.; Pandey, V., Srivastava, P. K.  
1180 (2021). Application of geospatial technology in agricultural water management. In:  
1181 *Agricultural Water Management*, 1 (1), 31-45. [https://doi.org/10.1016/B978-0-12-](https://doi.org/10.1016/B978-0-12-812362-1.00003-5)  
1182 [812362-1.00003-5](https://doi.org/10.1016/B978-0-12-812362-1.00003-5)

1183 Smith, RJ. (1993). Logarithmic transformation bias in allometry. *American Journal of*  
1184 *Physical Anthropology*, 90 (2), 215–228. <https://doi.org/10.1002/ajpa.1330900208>

1185 Souza, CM., Júnior., Z. Shimbo, J., Rosa, MR., Parente, LL., A. Alencar, A., Rudorff,  
1186 BFT., Hasenack, H., Matsumoto, M., G. Ferreira, L., Souza-Filho, PWM., de  
1187 Oliveira, SW., Rocha, WF., Fonseca, A.V., Marques, CB., Diniz, CG., Costa, D.,  
1188 Monteiro, D., Rosa, ER., Vélez-Martin, E., Weber, EJ., Lenti, FEB., Paternost, FF.,  
1189 Pareyn, FGC., Siqueira, JV., Viera, JL., Neto, LCF., Saraiva, MM., Sales, MH.,  
1190 Salgado, MPG., Vasconcelos, R., Galano, S., Mesquita, VV., Azevedo, T. (2020).  
1191 Reconstructing Three Decades of Land Use and Land Cover Changes in Brazilian  
1192 Biomes with Landsat Archive and Earth Engine. *Remote Sensing*, 12(17), 2735.  
1193 <https://doi.org/10.3390/rs12172735>

1194 Stahl, G., Saarela, S., Schnell, S., Holm, S., Breidenbach, J., Healey, SP., Patterson,  
1195 PL., Magnussen, S., Naesset, E., Mcroberts, RE., Gregoire, TG. (2016). Use of  
1196 models in large-area forest surveys: comparing model-assisted, model-based and  
1197 hybrid estimation. *Forest Ecosystems*, 3 (1), 1-11. [https://doi.org/10.1186/s40663-016-](https://doi.org/10.1186/s40663-016-0064-9)  
1198 [0064-9](https://doi.org/10.1186/s40663-016-0064-9)

1199 Staver AC, Archibald S, Levin SA. (2011). The global extent and determinants of  
1200 savanna and forest as alternative biome states. *Science*, 334 (6053), 230-232.  
1201 <https://doi.org/10.1126/science.1210465>

1202 Streutker, DR., Glenn, N. F. (2006). LiDAR measurement of sagebrush steppe  
1203 vegetation heights. *Remote Sensing of Environment*, 102 (1-2), 135-145.  
1204 <https://doi.org/10.1016/j.rse.2006.02.011>

1205 Sugiura, N. (1978). Further analysts of the data by akaike' s information criterion  
1206 and the finite corrections. *Communications in Statistics - Theory and Methods*, 7 (1),  
1207 13-26. <https://doi.org/10.1080/03610927808827599>

1208 Tang, H., Armston, J., Hancock, S., Marselis, S., Goetz, S., Dubayah, R. (2019).  
1209 Characterizing global forest canopy cover distribution using spaceborne lidar.  
1210 *Remote Sensing of Environment*, 231 (15), 111262.  
1211 <https://doi.org/10.1016/j.rse.2019.111262>

1212 Valbuena, R., O'connor, B., Zellweger, F., Simonson, W., Vihervaara, P., Maltamo,  
1213 M., Silva, CA., Almeida, DRA., Danks, F., Morsdorf, F., Chirici, G., Lucas, R.,  
1214 Coomes, DA., Coops, NC. (2020). Standardizing ecosystem morphological traits  
1215 from 3D information sources. *Trends in Ecology & Evolution*, 3 (8), 656-667.  
1216 <https://doi.org/10.1016/j.tree.2020.03.006>

1217 Van der Werf, GR., Randerson, JT., Giglio, L., Collatz, GJ., Mu, M., Kasibhatla, PS.,  
1218 Morton, D C, DeFries, RS., Jin, Y., Van Leeuwen, TT. (2010). Global fire emissions  
1219 and the contribution of deforestation, savanna, forest, agricultural, and peat fires  
1220 (1997-2009). *Atmospheric Chemistry and Physics*, 10 (23), 11707-11735.  
1221 <https://doi.org/10.5194/acp-10-11707-2010>

1222 Wang, C., Shu, Q., Wang, X., Guo, B., Liu, P., Li, Q. (2019). A random forest  
1223 classifier based on pixel comparison features for urban LiDAR data. *ISPRS journal*  
1224 *of photogrammetry and remote sensing*, 148 (1), 75-86.  
1225 <https://doi.org/10.1016/j.isprsjprs.2018.12.009>

1226 Wang, D., Xin X., Shao, Q., Brolly, M., Zhu, Z., Chen J. (2017). Modeling  
1227 Aboveground Biomass in Hulunber Grassland Ecosystem by Using Unmanned  
1228 Aerial Vehicle Discrete Lidar. *Sensors*, 17(1), 180. [https:// doi:10.3390/s17010180](https://doi:10.3390/s17010180)

1229 Wilcoxon, F. (1945). Individual comparisons of grouped data by ranking methods.  
1230 *Journal of economic entomology*, 39 (2), 269-270. <https://doi.org/10.1093/jee/39.2.269>

1231 Wilkinson, B., Lassiter, HA., Abd-Elrahman, A., Carthy, RR., Ifju, P., Broadbent, E.,  
1232 Grimes, N. (2019). Geometric targets for UAS lidar. *Remote Sensing*, 11 (24), 3019.  
1233 <https://doi.org/10.3390/rs11243019>.

- 1234 Zanne, A. E., Lopez-Gonzalez, G., Coomes, D. A., Ilic, J., Jansen, S., Lewis, S. L., ...  
1235 & Chave, J. (2009). Global wood density database. *Dryad*. Identifier:  
1236 <http://hdl.handle.net/10255/dryad.235>.
- 1237 Zhang, H., Sun, Y., Chang, L., Qin, Y., Chen, J., Qin, Y., ... & Wang, Y. (2018).  
1238 Estimation of grassland canopy height and aboveground biomass at the quadrat  
1239 scale using unmanned aerial vehicle. *Remote sensing*, 10 (6), 851.  
1240 <https://doi.org/10.3390/rs10060851>
- 1241 Zhao, K., Suarez, J. C., Garcia, M., Hu, T., Wang, C., Londo, A. (2018). Utility of  
1242 multitemporal lidar for forest and carbon monitoring: Tree growth, biomass  
1243 dynamics, and carbon flux. *Remote Sensing of Environment*, 204, 883-897.  
1244 <https://doi.org/10.1016/j.rse.2017.09.007>
- 1245 Zimbres, B., Shimbo, J., Bustamante, M., Levick, S., Miranda, S., Roitman, I.,  
1246 Alencar, A. (2020). Savanna vegetation structure in the Brazilian Cerrado allows  
1247 for the accurate estimation of aboveground biomass using terrestrial laser  
1248 scanning. *Forest Ecology and Management*, 458 (1), 117798.  
1249 <https://doi.org/10.1016/j.foreco.2019.117798>
- 1250